


# Geospatial mapping and multivariate statistical analysis for assessing groundwater quality in Bou Arada-El Aroussa plain, Northwestern Tunisia

## Mappatura e analisi statistica multivariata per valutare la qualità delle acque sotterranee nella Pianura di Bou Arada-El Aroussa, Tunisia Nord-Occidentale

Imed BEN SLIMENE<sup>a</sup>, Amor BEN MOUSSA<sup>a</sup> , Stefan GEYER<sup>b</sup>, Ismail TRABELSI<sup>c</sup>

<sup>a</sup> Research Laboratory of Environmental Sciences and Technologies, Higher Institute of Sciences and Technology of Environment of Borj Cedria, University of Carthage, University Campus of the Borj-Cedria Technopole BP 122, Hammam-Chott 1164, Tunisia, e-mail  : [amor.benmoussa@isste.ucar.tn](mailto:amor.benmoussa@isste.ucar.tn); [amor\\_geologie@yahoo.fr](mailto:amor_geologie@yahoo.fr)

<sup>b</sup> Department Catchment Hydrology, Helmholtz-Centre for Environmental Research, D-06120 Halle, Germany

<sup>c</sup> Center of Research and Technologies of Water (CERTe), Laboratory of Treatment and Recycle of wastewater, Tunisia.

### ARTICLE INFO

Ricevuto/Received: 7 October 2024

Accettato/Accepted: 13 February 2025

Publicato online/Published online:

30 March 2025

Handling Editor:

Marco Pola

### Citation:

Ben Slimene, I., Ben Moussa A., Geyer S., Trabelsi I., (2025). Geospatial mapping and multivariate statistical analysis for assessing groundwater quality in Bou Arada-El Aroussa plain, Northwestern Tunisia

Acque Sotterranee - *Italian Journal of Groundwater*, 14(1), 65 - 83

<https://doi.org/10.7343/as-2025-816>

### Correspondence to:

Amor Ben Moussa  :

[amor.benmoussa@isste.ucar.tn](mailto:amor.benmoussa@isste.ucar.tn)

**Keywords:** groundwater, irrigation water quality indices, multivariate analysis, GIS, Bou Arada-El Aroussa.

**Parole chiave:** acqua sotterranea, indici di qualità dell'acqua per scopi irrigui, analisi multivariata, GIS, Bou Arada-El Aroussa.

### Riassunto

Questo lavoro presenta uno studio integrato delle acque sotterranee nella pianura di Bou-Arada-El Arroussa per analizzare la loro qualità per scopi irrigui e la distribuzione spaziale. Il fine è di supportare gli organi decisionali nello sviluppo di piani di gestione sostenibile delle risorse idriche sotterranee. La valutazione della qualità dell'acqua effettuata in questo lavoro inizia con un'analisi statistica per determinare le analogie tra i campioni e raggrupparli in cluster. A ciò segue un'analisi delle componenti principali sui parametri fisico-chimici per determinare le relazioni tra le variabili e visualizzare la loro dipendenza mediante una matrice di correlazione. Le analisi statistiche combinate con un approccio grafico tramite i diagrammi Piper, Gibbs, Wilcox e USSL permettono di valutare in dettaglio le proprietà delle acque, le facies idrochimiche e le interazioni con la matrice dell'acquifero. Inoltre, sono stati utilizzati sistemi informativi geografici (GIS) per combinare meglio gli indici di qualità e creare una mappa della distribuzione spaziale della qualità delle acque. L'analisi dei cluster e l'analisi delle componenti principali evidenziano tre tipi di acqua. Il primo caratterizzato da una TDS elevata raggruppa insieme i campioni F04, F05 e P01. Il secondo tipo include solo il pozzo P23, distinto da contenuti elevati di  $K^+$ ,  $Mg^{2+}$  e  $NO_3^-$ . Il terzo tipo può essere ulteriormente suddiviso in due sottoinsiemi: uno caratterizzato da una composizione dominata dal  $SO_4^{2-}$  e l'altro da  $Cl^-$ , associato ad altri ioni come  $HCO_3^-$ ,  $Ca^{2+}$  e  $Na^+$ . Le analisi chimiche delle acque sotterranee di Bou Arada-El Arroussa mostrano che l'ordine di abbondanza degli ioni principali è  $SO_4^{2-} > Cl^- > HCO_3^- > Ca^{2+} > Mg^{2+} > NO_3^- > K^+$ . Il diagramma di Piper e i rapporti ionici hanno rivelato tre facies idrochimiche (Ca-Mg- $SO_4$ , mista e Na-Cl) in linea con i risultati ottenuti dal clustering. I campioni di acqua sono classificati tramite l'indice di durezza dell'acqua (TH) nella categoria di acqua dure e salmastre a causa del loro elevato contenuto di magnesio e calcio, che è cruciale per la crescita delle piante specialmente nelle aree agricole. L'analisi sulla relazione tra la composizione chimica delle acque e la composizione mineralogica del sistema acquifero rivela che tutti i campioni di acqua sotterranea rientrano nel campo corrispondente all'interazione acqua-roccia, ad eccezione di F04 e F05 che mostrano la predominanza di processi di evaporazione. Il diagramma di Chadha mostra che la maggior parte dei campioni si trova nella zona di scambio ionico inverso, suggerendo uno scambio tra acque sotterranee e minerali argillosi. Il diagramma USSL mostra che la maggior parte dei campioni appartiene alla categoria C3-S1, indicando che l'acqua non è adatta per l'irrigazione a causa dell'elevato contenuto salino. La valutazione della qualità dell'acqua per l'irrigazione ha rivelato che la maggior parte dei campioni è conforme agli standard per l'uso agricolo. Un'analisi multicriteri sui valori degli indici SAR, SSP, PS, RSC,  $Na\%$  e IWQI ha permesso di creare una mappa di sintesi della distribuzione spaziale della qualità dell'acqua. Questa mappa rivela che la parte occidentale della pianura di Bou-Arada El Arroussa contiene acqua di buona qualità, mentre la parte orientale contiene acqua di qualità inferiore legata alla risalita di acqua profonda di scarsa qualità.

### Abstract

*This paper presents an integrated study of groundwater quality for irrigation and its spatial distribution in the Bou-Arada-El Arroussa plain to guide decision-makers in the development of sustainable groundwater resource management plans. Assessing water quality for irrigation in this plain involves a process that begins with statistical analysis to determine similarities between samples and group them into clusters. This is followed by principal component analysis on physico-chemical data to determine relationships between variables and visualize their independence on a correlation matrix. Statistical analyses combined with a graphical approach through diagrams such as Piper, Gibbs, Wilcox and USSSL are used to better assess the properties, facies and interactions between water and minerals within the aquifer. In addition, geographic information system (GIS) tools were used to better combine water quality indices and create a map of spatial quality distribution. Clustering results and principal component analysis reveal three types of water: the first type includes samples F04, F05 and P01, characterized by high concentration of TDS. The second type consists solely of well P23, distinguished by elevated level of  $K^+$ ,  $Mg^{2+}$  and  $NO_3^-$  ions. The third type can be divided into two subsets: one dominated by  $SO_4^{2-}$  and the other by  $Cl^-$ , with additional ions such as  $HCO_3^-$ ,  $Ca^{2+}$  and  $Na^+$ . Major ions analyses of the Bou Arada-El Arroussa groundwater show that the order of ions abundance was  $SO_4^{2-} > Cl^- > HCO_3^- > Ca^{2+} > Mg^{2+} > NO_3^- > K^+$ . Piper diagrams and ion ratios revealed three water facies similar to the results obtained from the cluster analysis dendrogram: Ca-Mg- $SO_4$ , mixed and Na-Cl facies. The water hardness index (TH) classifies water samples into hard-brackish water category due to their high magnesium and calcium contents, which is crucial for plant growth especially in agricultural area. The investigation of the relationship between water chemistry and mineralogical composition of the studied aquifer system reveals that all groundwater samples fall in the field corresponding to the water-rock interaction, with the exception of F04 and F05 showing a predominant evaporation. The Chadha diagram shows that the majority of samples are located in the reverse ion exchange zone reflecting the exchange between groundwater and clay minerals. The USSSL diagram shows that the majority of samples belong to the C3-S1 category, reflecting that the water is not suitable for irrigation due to the high salinity content. Evaluation of irrigation water quality using quality indices revealed that the majority of samples are within the standards for agricultural use. A multi-criteria analysis on the indices layers (SAR, SSP, PS, RSC, Na% and IWQI) created a synthesis map of the spatial distribution of the water quality. This map reveals that the western part of the Bou-Arada El Arroussa plain contains good-quality water, while the Eastern part contains the poorest quality related to the upwelling of poor-quality deep water.*

### Introduction

In the arid and semi-arid regions of the Southern Mediterranean, climate change has intensified pressure on water resources. This involves increased temperatures, decreased rainfall, and more frequent droughts, which disrupt the precarious balance of water resources (Mehta et al., 2024; Surkar & Choudhary, 2023). This change, combined with anthropogenic activities, has led to declining piezometric levels and the deterioration in groundwater quality (Abdelfattah et al., 2023; Besser et al., 2019; Gautam et al., 2022; Wu & Sun, 2016).

In agricultural regions, water is the key component of any sustainable development plan. Thus, the assessment and management of groundwater resources have been the subject of various methodological approaches. Methods based exclusively on hydrochemical analysis are limited in their ability to understand the complex interactions between different parameters (Appelo & Postma, 2005). Isotopic techniques, while effective in tracing the origin and recharge processes of aquifers, remain costly and technically complex (Clark & Fritz, 1997). Multivariate statistical methods, such as Principal Component Analysis (PCA) and Cluster Analysis (CA), can identify relationships between hydrochemical variables, but require large databases (Gadelha et al., 2023; Su et al., 2023). The integration of GIS tools with statistical methods has enabled better spatial visualization of results (Bakr, 2013; Bordbar et al., 2023; R. Li et al., 2024; Radmehr et al., 2022). In addition, coupled hydrochemical and isotopic approaches

have improved the understanding of mineralization processes (Rel Dechangue & Kabeyene Veronique, 2023; Salem et al., 2023). Finally, irrigation water quality indices (IWQIs) can be used to assess the suitability of groundwater for agricultural use (Abidi et al., 2024; Asma & Şener, 2024; Mandloi et al., 2024). However, few studies propose an integrated approach combining these different methodologies.

In this context, the Bou Arada-El Aroussa plain (BAEA), located in North-western Tunisia, is a relevant case study. This region hosts a major multi-layer aquifer system with a marked diversity of soil types, including rendzina and calcareous brown soils (44%), poorly developed mineral soils (23%) and complex soils (23%) (CRDA, 2004). Irrigation with poor-quality water in this type of environment can lead to increased salinization of the soil, reduced fertility and degradation of its structure (Kramer & Mau, 2023; Zhang et al., 2024).

This study proposes an innovative methodological approach that combines multiple techniques to understand the aquifer's geometry, hydrodynamics and water quality. The methodology integrates:

- Multivariate statistical analysis implemented in Python including CA and PCA to identify geochemical processes.
- Water quality indices calculations to assess irrigation water suitability.
- The Chadha diagram to identify hydrochemical evolution and the Gibbs graph to examine water chemistry relationships (Chadha, 1999; Sun et al., 2021).

- GIS mapping for spatial visualization of results.

This integrated approach makes it possible to correlate physico-chemical parameters, identify similarities between samples and reveal processes influencing groundwater quality (Adawe et al., 2024; Garba et al., 2023; Mecibah et al., 2024; Salem et al., 2023).

The major purpose of the present investigation is to provide scientific data on the hydrodynamic functioning and the geochemical processes that impact water quality in the BAEA aquifer system. This study addresses three key aspects: (i) understanding the geometry, structure and hydrodynamics of the BAEA aquifer system; (ii) assessing the impact of natural and anthropogenic activities on water quality; and (iii) highlighting the main hydrochemical processes that control the quality of the waters studied. The expected results will contribute to a better understanding of the BAEA plain aquifer system, by characterizing its structure, hydrogeological dynamics and the factors influencing groundwater quality. The study also aims to provide managers with a decision-making tool for sustainable water resource management in a context of climate change. It stands out for its integrated, multidisciplinary approach, offering a robust, reproducible assessment that can be applied to other aquifer systems in similar environments.

## Materials and Methods

### Study area

The plain of BAEA (Fig. 1), which is located northwest of Tunisia in the governorate of Siliana, is 35 km long and 5 km wide. It is located between latitudes 36°7'31" to 36°34'38" north and longitudes 9°8'2" to 9°57'24" east (Mahjoub & Dali, 1998; Dali, 1994; Perthuisot, 1970; Jausein & Berthe, 1961).

### Geological and Hydrogeological Setting

Geologically, BAEA plain is characterized by a succession of sedimentary units ranging from the Lower Cretaceous to the Quaternary (Fig. 2). The Lower Cretaceous deposits, which outcrop west and east of Jebel Er Rihan, can reach a thickness of approximately 700 meters and consist of marl, marly limestone and limestone (Arfaoui et al., 2018; Ben Chelbi et al., 2013; Ben Yagoub, 1979). The Upper Cretaceous deposits are composed of nodular limestones, followed by clays and marly shales, overlain by black marls and stratified limestones (Arfaoui et al., 2018; Ben Chelbi et al., 2013; Jausein & Berthe, 1961; Mahjoub & Dali, 1998). These are in turn overlain by yellowish marls and intercalation of marls and limestones of the El Haria Formation observed to the west of the plain and at Koudiat Tarf ech Chena and Sidi Slem. Lower Eocene sediments consist of a thin basal layer of glauconitic and phosphatic limestone, followed by thinly bedded limestone alternating with gray marls. The Middle Eocene, sometimes overlain by Oligocene sediments, is composed of thin layers of deltaic sandstone outcropping in the northern part of the plain, between Sidi ed Dakhli and Kat Sidi Barka, and in the southern part of the plain, between Oued Er Rmil and Oued El Melah (Arfaoui et al., 2018; Mahjoub & Dali, 1998). The Upper Eocene outcrops at Jebel Bessioud west of the Djelida station and in the region of Sidi Ali Ben Al are characterized by yellow clays and lumachels levels with very rare limestone interlayers. The Oligocene series, composed of sands and conglomerates, crops out in the Oued Er Rmil syncline, between Sidi Nsib and Sidi Jaber and is unconformably overlain by the Miocene-Pliocene continental detrital series. Finally, Quaternary deposits, composed of red limestone, conglomerates and limestone crusts, silts, sandy clays and gypsum, crop out in the form of terraces along the wadis and aeolian dunes around Sebkhet El Kourzia and Garaet El Hamada.

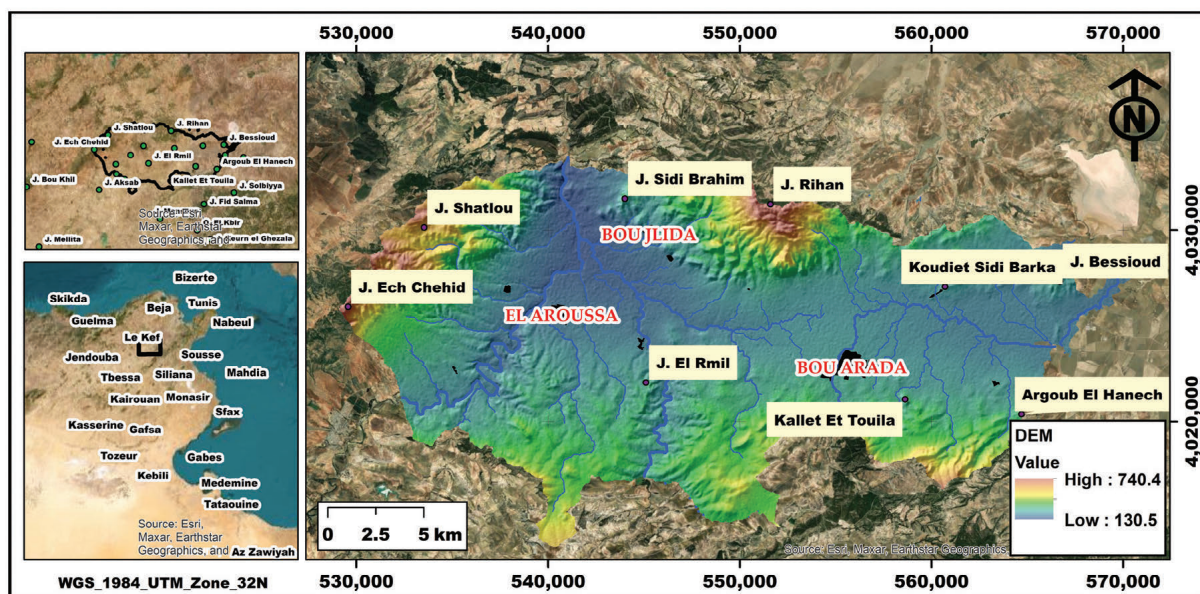


Fig. 1 - Location map of the Bou Arada-El Aroussa study area.

Fig. 1 - Carta dell'area di studio di Bou Arada-El Aroussa.



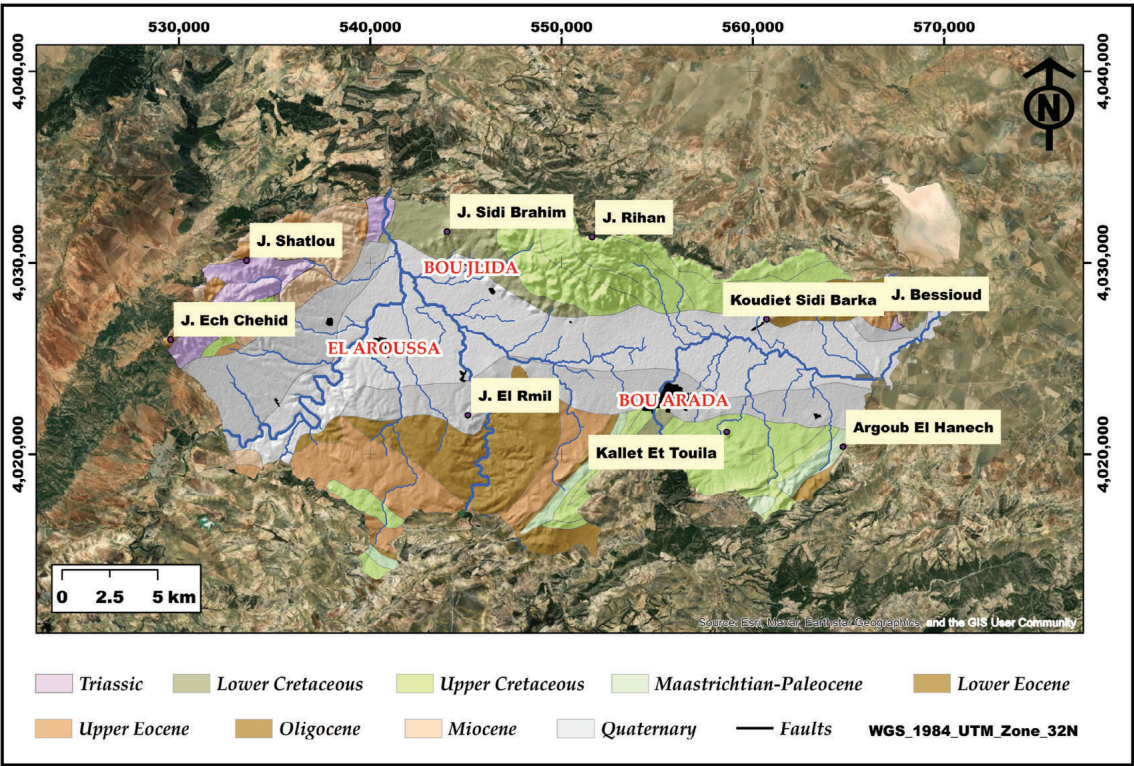


Fig. 2 - Detailed geological map of the BAEA study area (Mahjoub & Dali, 1998).

Fig. 2 - Carta geologica di dettaglio dell'area di studio (Mahjoub & Dali, 1998).

Hydrogeologically, the BAEA plain hosts two aquifers (Fig. 3), separated by a NW-SE fault. This fault is probably responsible for the formation of an eastern compartment (Bou Arada) characterized by an irregular faulted bedrock. The bedrock consists of Paleocene-age clays and marls attributed to the El Haria Formation (Fig. 4), organized as a horst and graben structure. The western compartment is a syncline with bedrock formed by Lutetian-Priabonian clays and marls (Fig. 4) attributed to the Souar Formation (Amri, 1992; Azzouz, 1988; Oueslati, 1990).

The Bou Arada (BA) compartment hosts a multi-layered aquifer, including a shallow aquifer in Quaternary deposits

and two deep aquifers in Quaternary deposits and Eocene limestones (Fig. 4). The total thickness can reach up to 700 meters in the center of the plain. The El Aroussa (EA) compartment hosts an aquifer situated in Oligocene sandstones, with a thickness reaching 300 meters at Oued El Melah (Amri, 1992; Azzouz, 1988; Boukhalfa et al., 2020; Dali et al., 1999; Oueslati, 1990).

The aquifer systems are recharged through the direct infiltration of rainwater on the surrounding hill faces and by indirect recharge along the numerous wadis that drain the aquifer. The estimated resources of these two systems can reach 5 Mm<sup>3</sup>/year, assuming an average rainfall of

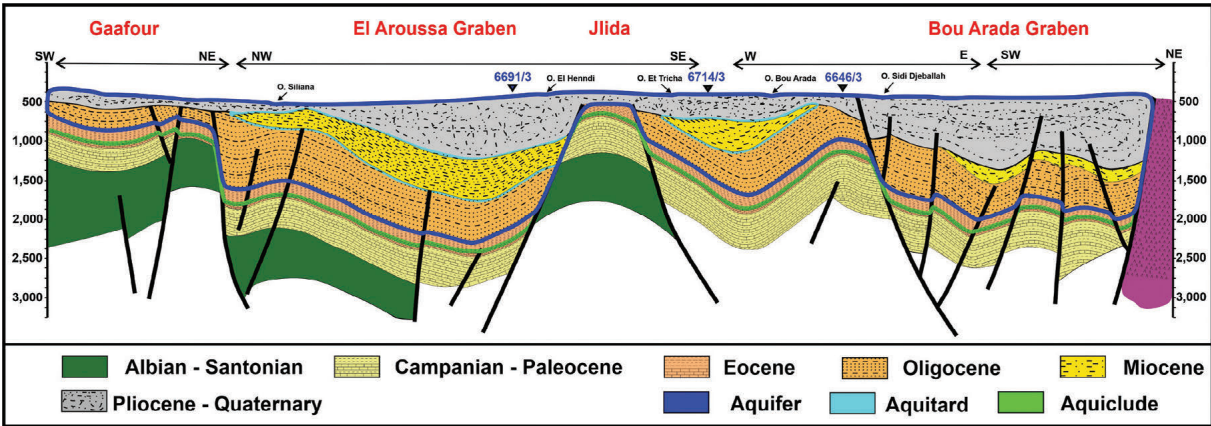


Fig. 3 - Geological section shows the hydrogeological unit boundaries in the Bou Arada-El Aroussa plain (Arfaoui et al., 2018).

Fig. 3 - Sezione geologica che riporta i limiti delle unità idrogeologiche nella pianura di Bou Arada-El Aroussa (Arfaoui et al., 2018).



Age	Formation	Lithology	Hydrogeological Unit	Aquifer Systems
QUATERNARY				
PALEOCENE	PIACENZIAN			El Krib Sidi Bou Rouls, Sers, Ras El-Maa, Bou Arada
	ZANCLEAN			
MIOCENE	MESSINIAN			Ras El-Maa
	TORTONIAN			
	SERRAVALLIAN			
	LANGHIAN			
	BURDIGALIAN			
OLIGOCENE	CHATTIAN			Gaafour, El Krib, O. Rmil, Oussletia
	RUPELIAN			
EOCENE	PRIBONIAN			Massouge, Bou Arada
	BARTONIAN			
	LUTETIAN			
PLIOCENE	YPRESIAN			Massouge, Bou Arada
	THANETIAN			
CRETACEOUS	DANIAN			Lakhouat, Gaafour, Massouge
	MAASTRICHTIAN			
	CAMPANIAN			
	SANTONIAN			
	CONIACIAN			
	TURONIAN			
	CENOMANIAN			
	ALBIAN			
	APTIAN			
	BARREMIAN			
TRIASSIC	HAUTERIVIAN			Bargou, Sodga, O. Ousafa, Serj
	VALANGINIAN			
	BERRIASIAN			

Fig. 4 - Litho-stratigraphy and potential hydrogeological units of the Bou Arada-El Aroussa plain (Ben Chelbi et al., 2013).

Fig. 4 - Successione litostratigrafica e potenziali unità idrogeologiche della pianura di Bou Arada-El Aroussa (Ben Chelbi et al., 2013).

400 mm/year and an effective infiltration rate of 5% (Fersi, 1979). The exploitation of these aquifer systems was estimated at 0.763 Mm<sup>3</sup>/year in 2019, equivalent to 24 L/s (DGRE, 2019) with 96% of the volume coming from the BA aquifer and 52% from the deep levels.

Wide variations in grain size, impermeable deposit thickness and abundance contribute to significant hydrodynamic variability, as illustrated by transmissivity values ranging from  $3.6 \times 10^{-6}$  to  $1.83 \times 10^{-2}$  m<sup>2</sup>/s and specific flow rates measured at different sites varying from 0.11 to 2.8 L/s (Amri, 1992; Azzouz, 1988; Oueslati, 1990).

In March 2022, water levels measured in 15 wells, referenced to sea level, were used to establish the piezometric map of the BAEA aquifer (Fig. 5). The piezometric map shows that the measured water levels vary from 280 m.a.s.l in the northern part of the basin to 240 m.a.s.l in the eastern and western parts of the study area. This may reflect that the general direction of groundwater flows for the Bou Arada aquifer system diverges towards the Oued Bou Arada to the east and the Oued Er Rmil to the west. Divergent NW-SE flow directions were observed for the Er Rmil aquifer system, indicating that the main recharge zones are located at the foot of the Djebel Er Riham and Sidi Bou Baker mountains and in the Oued Er Rmil syncline.

### Sampling and Analysis

In August 2023, a sampling campaign was carried out on the BAEA plain to collect 11 water samples in 500 ml polyethylene bottles, including 8 from boreholes and 3 from wells.

Physico-chemical parameters including temperature (T), pH, and electrical conductivity (EC) were measured in situ using a multiparameter HQ40D portable multi-parameter (Hach) (User Manual HQd Portable Meter, 2020). The geographical position of the samples, including latitude, longitude, and altitude, was recorded using a GPS unit.

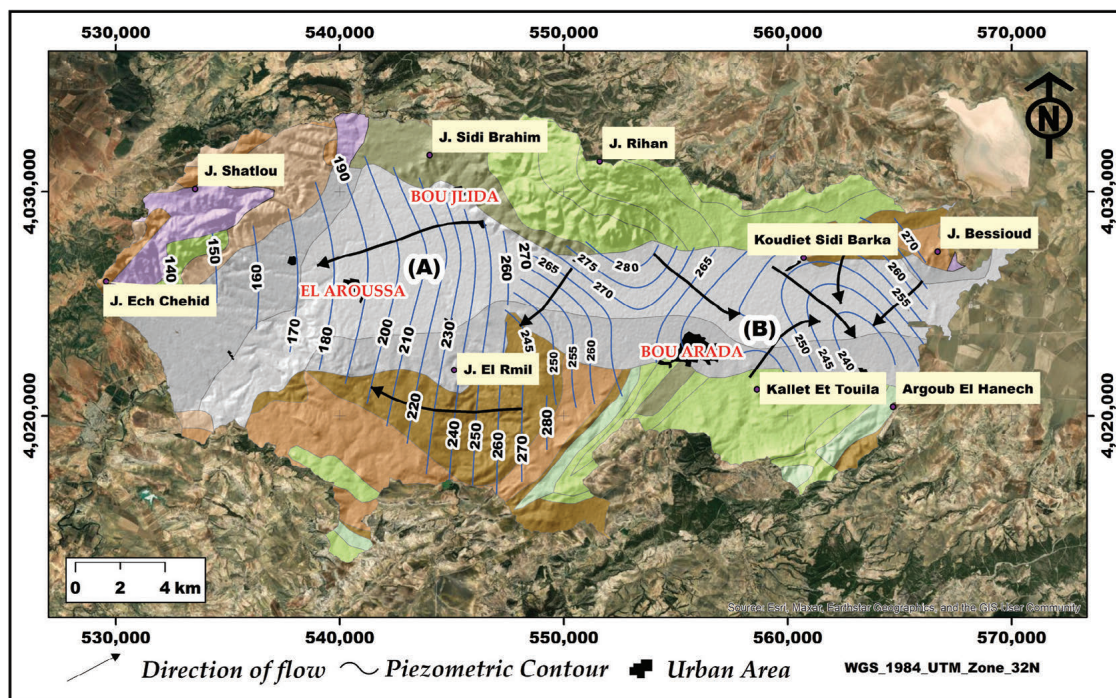


Fig. 5 - Piezometric maps for the year 2022 drawn up using 15 monitoring points: (A) Er Rmil piezometric map; (B) Bou Arada piezometric map.

Fig. 5 - Mappe piezometriche dell'area di Er Rmil (A) e Bou Arada (B) per l'anno 2022 ottenute utilizzando 15 punti di monitoraggio.

Water samples were collected at each site and prepared differently for future analysis: filtered at 0.2  $\mu\text{m}$  and 0.45  $\mu\text{m}$  using cellulose acetate filters (Sartorius Stedim Biotech GmbH, Göttingen, Germany), partially acidified with suprapur nitric acid (Merck) or left in their original state.

Dissolved concentrations of major elements ( $\text{Ca}^{2+}$ ,  $\text{Mg}^{2+}$ ,  $\text{Na}^+$ , and  $\text{K}^+$ ) in filtered and acidified samples were measured by inductively coupled plasma optical emission spectrometry (ICP-OES, Optima 7300 DV, PerkinElmer) in accordance with DIN EN ISO 11885.  $\text{Cl}^-$  and  $\text{SO}_4^{2-}$  were determined from filtered but not preserved part of the sample by ion chromatography with a Thermo Fisher ICS-6000 HPICTM suppressor system following the EN ISO 10304-4:1999 standard. Filtered samples were also analyzed for  $\text{NO}_3^-$ ,  $\text{NO}_2^-$  and  $\text{NH}_3^-$  with a Continuous-Flow Analyzer (SFA) San++ from Skalar applying the methods specified in DIN EN ISO 13395, DIN EN ISO 11732 and DIN EN ISO 15681-2.

The  $\text{HCO}_3^-$  concentration was determined by titration, using 0.05 mol hydrochloric acid and a pH meter as a steady-state indicator. An ion balance check confirmed an acceptable margin of error of less than 5%, in accordance with the standard of (Baird & Eaton, 2017).

The necessary quality of analytical data was ensured by regular method validations and successful participation in annual intercomparison tests in the laboratories of the (UFZ) Helmholtz-Centre for Environmental Research in Halle.

## Indexing Approach

### Chloro-Alkaline Indexes (CAIs)

The origin and geochemical processes affecting groundwater are determined using CAIs (Hartanto & Lubis, 2023). These indices are calculated from the concentrations of  $\text{Cl}^-$ ,  $\text{Na}^+$ ,  $\text{SO}_4^{2-}$  and sometimes  $\text{K}^+$  ions.

In conjunction with other geochemical parameters, CAIs provide a comprehensive understanding of the origin and evolution of groundwater. They can also identify areas affected by saltwater intrusion or the dissolution of evaporitic minerals. The principle is simple: water of marine or evaporitic origin has higher  $\text{Cl}^-/\text{Na}^+$  ratios than meteoric water. There are several CAIs, each with its advantages for interpreting ion exchange. They are calculated using concentrations expressed in meq/L, according to the following formulae:

$$\text{CAI-I} = \frac{\text{Cl}^- - (\text{Na}^+ + \text{K}^+)}{\text{Cl}^-} \quad (1)$$

$$\text{CAI-II} = \frac{\text{Cl}^- - (\text{Na}^+ + \text{K}^+)}{\text{SO}_4^{2-} + \text{HCO}_3^- + \text{CO}_3^{2-} + \text{NO}_3^-} \quad (2)$$

### Irrigation Water Quality indices (IWQIs)

IWQIs combine several physical, chemical and biological parameters to assess the quality of water used for irrigation (Tab. 1). These indices have proved useful for assessing and managing soil resources and agricultural production. They

can be used to assess the potential impact of irrigation water quality on soil properties and crop yields (Singh et al., 2020; Thapa et al., 2020). Indices such as IWQI, SAR, Na%, SSP, PS and RSC were calculated from the physico-chemical characteristics of groundwater samples collected in the study area, as shown in Table 1. The unit of concentration used in the calculations is meq/L, with the exception of the IWQI,

Tab. 1 - IWQIs equations and references.

Tab. 1 - Equazioni per ottenere IWQIs e referenze.

IWQI	Formula	References
SAR	$\text{SAR} = \left( \frac{\text{Na}^+}{\sqrt{\frac{(\text{Ca}^{2+} + \text{Mg}^{2+})}{2}}} \right) \times 100$	(Richards, 1954)
Na%	$\text{Na\%} = \left( \frac{\text{Na}^+ + \text{K}^+}{(\text{Ca}^{2+} + \text{Mg}^{2+}) + (\text{Na}^+ + \text{K}^+)} \right) \times 100$	(Ravikumar et al., 2013)
SSP	$\text{SSP} = \left( \frac{\text{Na}^+}{\text{Ca}^{2+} + \text{Mg}^{2+} + \text{Na}^+} \right) \times 100$	(Eaton, 1950)
PS	$\text{PS} = \text{Cl}^- + \left( \frac{\text{SO}_4^{2-}}{2} \right)$	(Doneen et al., 1964)
RSC	$\text{RSC} = (\text{HCO}_3^- + \text{CO}_3^{2-}) - (\text{Ca}^{2+} + \text{Mg}^{2+})$	(Eaton, 1950)

which is calculated in mg/L.

The Irrigation water quality index (IWQI) is then calculated using equation (3) in Table 1, where each parameter is weighted by its corresponding weight (Meireles et al., 2010).

$$\text{IWQI} = \sum_{i=1}^n Q_i \times W_i \quad (3)$$

The values of the parameters ( $Q(\text{EC})$ ,  $Q(\text{SAR})$ ,  $Q(\text{Cl}^-)$ ,  $Q(\text{Na}^+)$ ,  $Q(\text{HCO}_3^-)$ ) are represented by  $Q_i$ , and the weight associated with each parameter are represented by  $W_i$ .

The different  $Q_i$  variables are standardized by equation (4) on a scale of 0 to 100, enabling them to be combined to obtain an overall water quality index (Tab. 2).

$$Q_i = Q_{\max} - \left( \frac{[(x_{ij} - x_{\inf}) \times Q_{\text{amp}}]}{x_{\text{amp}}} \right) \quad (4)$$

$x_{\inf}$ : the value corresponding to the lower limit of the class

$x_{ij}$ : the value observed for each variable

$Q_{\text{amp}}$ : the amplitude of the class

$x_{\text{amp}}$ : the amplitude of the class in which the variables fall

The parameter weights ( $W_i$ ) are calculated in Python, following a PCA on a set of physico-chemical parameters. Data for the selected parameters ( $Q(\text{SAR})$ ,  $Q(\text{HCO}_3^-)$ ,  $Q(\text{Na})$ ,  $Q(\text{Cl})$  and  $Q(\text{EC})$ ) are standardized, then a PCA is performed

Tab. 2 - Reference limits of values for the variables used to calculate the  $Q_i$  in Equation (4) (Salem et al., 2023).Tab. 2 - Limiti di riferimento per le variabili utilizzate nel calcolo di  $Q_i$  nell'Equazione (4) (Salem et al., 2023).

$Q_i$	SAR	EC ( $\mu\text{S/cm}$ )	$\text{HCO}_3^-$ (meq/L)	$\text{Na}^+$ (meq/L)	$\text{Cl}^-$ (meq/L)
0-35	$\text{SAR} > 2$ or $\text{SAR} \geq 12$	$\text{EC} < 200$ or $\text{EC} \geq 3,000$	$\text{HCO}_3^- < 1$ or $\text{HCO}_3^- \geq 8.5$	$\text{Na}^+ < 2$ or $\text{Na}^+ \geq 9$	$\text{Cl}^- < 1$ or $\text{Cl}^- \geq 10$
35-60	$6 \leq \text{SAR} < 12$	$1,500 \leq \text{EC} < 3,000$	$4.5 \leq \text{HCO}_3^- < 8.5$	$6 \leq \text{Na}^+ < 12$	$7 \leq \text{Cl}^- < 10$
60-85	$3 \leq \text{SAR} < 6$	$750 \leq \text{EC} < 1,500$	$1.5 \leq \text{HCO}_3^- < 4.5$	$3 \leq \text{Na}^+ < 6$	$4 \leq \text{Cl}^- < 7$
85-100	$2 \leq \text{SAR} < 3$	$200 \leq \text{EC} < 750$	$1 \leq \text{HCO}_3^- < 1.5$	$2 \leq \text{Na}^+ < 3$	$1 \leq \text{Cl}^- < 4$

to obtain the principal components and their respective explained variances. The raw weights of the variables are then calculated for each principal component. These raw weights are then normalized by dividing them by their sum to obtain relative weights. This calculation of normalized weights enables us to identify the most influential variables on the data set.

### Cluster Analysis

Cluster analysis is a powerful technique for processing water chemistry data. Methods such as hierarchical clustering (Ward, 1963) and the Elbow method (Onumanyi et al., 2022) can provide information on the variation in water quality and identify groups of samples. The clustering of groundwater samples showing common characteristics helps us to understand geological variations, variations in water quality, sources of pollution and hydrogeological processes necessary for the sustainable management of water resources (Gallardo Ceron et al., 2023; X. Li, 2023; Narvaez-Montoya et al., 2023; Pham & Nguyen, 2024).

The Ward method used in this study differs from the other techniques since it employs an analysis of variance (ANOVA) to assess the distances between groups calculating the sum of squared errors that reflects the total distance of each data point from the centroid of its parent group. Ward's method proves effective in producing an approximate solution to the clustering problem (Ward, 1963).

All hierarchical clustering analysis was performed in Python, using the SciPy library (Virtanen et al., 2020) for dendrogram calculation. The process begins by normalizing the physico-chemical variables of the study area using scikit-learn's StandardScaler (Pedregosa et al., 2011). Then, using Euclidean distance, a distance matrix is calculated, followed by hierarchical clustering using Ward's method.

The clustering results are visualized using a dendrogram, which shows the tree structure of the groups formed as a function of the similarity between samples. Similarity is deduced from a measure of the distance between samples, as a Euclidean distance.

### Factorial Analysis (FA) and Principal Component Analysis (PCA)

A factorial analysis (FA) was performed to estimate the weights of the physicochemical parameters (EC,  $\text{Na}^+$ ,  $\text{HCO}_3^-$ ,  $\text{Cl}^-$ , SAR), necessary for calculating the IWQI. This process begins with a CLR (Centered Log-Ratio) transformation to ensure data coherence and reliability, followed by the

standardization of the value to enable comparability scale across parameters (Sunkari et al., 2020; Smida et al., 2010)

Principal component analysis (PCA), a powerful statistical technique widely used in hydrochemical studies of groundwater quality, was then applied to reduce the dimensionality of the data. This reduction facilitates the analysis of complex hydrochemical datasets and reveals hidden relationships between geochemical variables (Gadelha et al., 2023; Hasbaia et al., 2021; Salman Dawood et al., 2018).

The PCA approach groups water samples according to their hydrochemical similarities and identifies factors responsible for variation in water quality by testing different parameters. Eigenvalues and eigenvectors derived from PCA were used to determine the relative importance of each physicochemical parameter. Libraries such as SciPy, scikit-learn, Matplotlib (Hunter, 2007) and factor\_analyzer were used to perform the analysis. The data are normalized, and a correlation matrix is calculated and visualized as a heatmap to assess relationships between variables. Additionally, Kaiser-Meyer-Olkin (KMO) indices and Bartlett's test of sphericity are calculated to assess the suitability of the data for PCA.

The weights ( $W_i$ ) of the parameters were calculated from the eigenvalues of the principal components, with an adjustment to ensure that their sum equals 1 (Yıldız & Karakuş, 2020). This robust methodology aggregates multiple physicochemical parameters into a comprehensive evaluation of irrigation water quality indices, using the Python tools.

### Geospatial analysis

Water quality indices for irrigation are essential for decision-makers when drawing up sustainable resource management plans. However, the sheer number of indices (6 in this study) and the difficulty of interpreting their values, especially for non-specialists in the field, make them difficult to evaluate. In this context, a raster aggregation analysis is carried out using ArcMap software (ESRI, 2020; Jain & Singh, 2022; Ouhakki et al., 2024). The water quality indices are interpolated by the IDW (Inverse Distance Weighting) with barrier tool to avoid having superfluous values that exceed our working range determined by the calculated values. Once the map is ready, it is reclassified using the classes determined for each index and weighting ranging from 5 (Excellent) to 1 (Poor) is assigned to define the quality classes. Once the new reclassified maps have been obtained, a merging operation is performed using Raster Calculator following a summation formula to create the new map synthesizing the data from these indices.



Results and Discussion

Groundwater Hydrochemical Properties

Water samples from the BAEA aquifer system were classified according to their physico-chemical properties and ionic species, referring to FAO and WHO standards (Tab. 3) (Zhu et al., 2023).

The pH values of the groundwater samples range from 7.10 to 7.82, with an average of 7.40 indicating that all water samples were alkaline and in accordance with the current standards of 6.5 to 8.4 for water use in irrigation.

The water hardness index (TH) was studied in conjunction with the total dissolved solids (TDS). This approach provided a comprehensive characterization of the water quality in the study area (Fig. 6). The TDS/TH diagram shows that TDS and TH values vary widely from 1,322 to 5,249 mg/L and from 519.62 to 3,211.62 mg/L, respectively. All groundwater samples are classified as hard brackish water due to their high magnesium and calcium contents, which are crucial for plant growth, especially in agricultural areas. However, these very hard waters can cause scale to precipitate in irrigation systems, trap plant roots, and form solid structures that prevent the absorption of other nutrients added to fertilizers (Karar & Henni, 2020; Pierret & Moran, 2011).

The electrical conductivity values of 9 groundwater samples, representing 82% of the total sampled water, are below the FAO of 3000  $\mu\text{S}/\text{cm}$ . However, groundwater samples collected from F05 and P01 boreholes, located north of Sidi Ayyed towards the downstream part of the plain, exhibit high conductivity values. This suggests either the influence of salt dissolution processes or the infiltration of irrigation water.

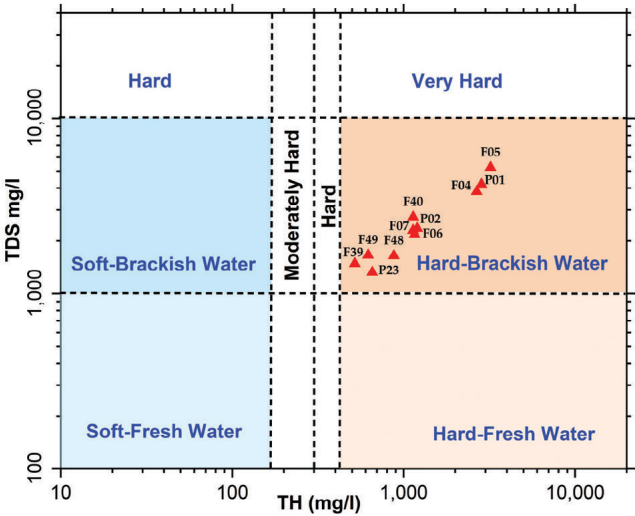


Fig. 6 - Diagram of TDS vs TH.  
Fig. 6 - Diagramma della TDS e TH.

The trend of anion concentrations was as follows:  $\text{SO}_4^{2-} > \text{Cl}^- > \text{HCO}_3^-$ , with average concentrations of 678.40, 604.27, and 448.97 mg/L, respectively. The pattern for cation concentrations was  $\text{Ca}^{2+} > \text{Na}^+ > \text{Mg}^{2+}$ , with mean concentrations of 379.18, 275.73 and 123.88 mg/L, respectively (Tab. 3 (A)). These relatively high concentrations may be a result of natural water-rock interaction processes, namely the dissolution of evaporites, carbonates, and/or cationic exchanges process with clay minerals (Guo et al., 2023). In addition, the higher concentrations of  $\text{Ca}^{2+}$  and  $\text{SO}_4^{2-}$  that were measured in the F04 and F05 wells situated

Tab. 3 - Physico-chemical parameters of samples, water quality indices, descriptive statistic results, and standard limit of irrigation activity.  
Tab. 3 - Parametri fisico-chimici dei campioni, indici di qualità dell'acqua, risultati della statistica descrittiva e valori legislativi di riferimento per l'utilizzo delle acque a scopo irriguo.

ID	EC ( $\mu\text{S}/\text{cm}$ )	T (°C)	pH	Concentration in mg/L								
				$\text{Ca}^{2+}$	$\text{Mg}^{2+}$	$\text{Na}^+$	$\text{K}^+$	$\text{HCO}_3^-$	$\text{Cl}^-$	$\text{SO}_4^{2-}$	$\text{NO}_3^-$	TDS
F04	2,250	24.40	7.10	719.00	212.00	145.00	9.45	951.06	304.00	1,450.00	10.23	3,818.00
F05	3,450	24.80	7.23	864.00	256.00	312.00	6.54	1,142.86	1,250.00	1,260.00	129.17	5,249.00
F06	1,762	24.10	7.17	297.00	101.00	138.00	8.92	237.00	487.00	587.00	148.51	2,171.00
F07	1,937	26.30	7.69	339.00	69.70	268.00	6.22	213.86	421.00	940.00	20.45	2,292.00
P01	3,410	24.10	7.27	764.00	228.00	356.00	6.28	196.47	1,230.00	1,270.00	131.70	4,209.00
P02	1,837	21.60	7.50	217.00	160.00	330.00	3.69	496.89	518.00	514.00	100.42	2,354.00
F39	1,462	22.30	7.43	123.00	51.60	283.00	4.06	312.71	433.00	217.00	54.00	1,482.00
F40	2,300	23.80	7.20	280.00	106.00	483.00	3.02	431.08	593.00	735.00	95.27	2,736.00
F48	1,482	20.70	7.55	264.00	52.80	206.00	3.48	349.29	559.00	68.50	138.09	1,644.00
F49	1,455	23.10	7.45	136.00	68.20	340.00	5.33	339.56	484.00	209.00	73.51	1,659.00
P23	1,192	23.00	7.82	168.00	57.40	172.00	1.59	267.86	368.00	212.00	69.19	1,322.00
Minimum	1,192	20.70	7.10	123.00	51.60	138.00	1.59	196.47	304.00	68.50	10.23	1,322.00
Maximum	3,450	26.30	7.82	864.00	256.00	483.00	9.45	1,142.00	1,250.00	1,450.00	148.51	5,249.00
Average	2,048.82	23.47	7.40	379.18	123.88	275.73	5.32	448.97	604.27	678.40	88.23	2,630.54
Standard Deviation	762.35	1.56	0.23	269.40	76.77	104.68	2.45	312.00	324.85	491.26	47.24	1,269.64
FAO*	3,000		8.50	400.00	60.00	919.00	2.00	610.00	1,036.00	960.00	50.00	2,000.00



north of Sidi Ayyed region highlight the effect of the Triassic deposits that outcrop in Jebel Ech Chehid, north-west of the study area. The BAEA groundwater samples show  $\text{Na}^+$  and  $\text{K}^+$  levels that range from 138 to 483 mg/L, from 1.59 to 9.45 mg/L, respectively. The high contents of these cations, which still fall within the FAO threshold, were found south of Jebel Ech Chehid and around the irrigated areas of Er Rmil and El Arroussa reflecting the effect of dissolution of feldspars and the infiltration of irrigation water (Zoller et al., 1980).

The calcium cation concentrations, which vary widely from 123 to 864 mg/L, increase from east to west towards the Triassic deposits that crop out in the Ech Chehid Mountain. The concentration of  $\text{Ca}^{2+}$  in three samples is higher than irrigation standards, which could be indicative of the effect of gypsum dissolution and dedolomitization (Schoenherr et al., 2018; Bischoff et al., 1994). Groundwater samples show  $\text{Mg}^{2+}$  concentrations ranging from 51.60 to 256 mg/L, with an average of 123.88 mg/L, suggesting that about 73% of them exceed the irrigation standard, estimated to 60 mg/L. The highest  $\text{Mg}^{2+}$  concentrations are observed around Jebel Ech Chehid. This spatial distribution reflects two key factors: (1) the alteration of ferruginous minerals deriving from the Triassic deposits, which release  $\text{Mg}^{2+}$  into groundwater, and (2) the influence of the fault which facilitates the circulation of  $\text{Mg}^{2+}$ -rich fluids through fractures and enhances its concentrations in the aquifer (Henchiri et al., 2015; Hamzaoui-Azaza et al., 2012). The bicarbonate concentration in the BAEA plain varies from 196.47 to 1142 mg/L, with an average of 448.97 mg/L. The majority of groundwater samples show  $\text{HCO}_3^-$  contents below the irrigation threshold, with the exception of two boreholes (F04 and F05) located on

the southern edge of Jebel Ech Chehid.

$\text{Cl}^-$  concentrations, which vary from 304 to 1250 mg/L, with an average of 604.27 mg/L, are below the irrigation standard. There were only two samples collected from P01 and F05 that showed slightly higher concentrations than the irrigation standard. Groundwater samples exhibits  $\text{SO}_4^{2-}$  contents that vary largely from 68.50 to 1450 mg/L, with only three samples (F04, F05, and P01) that exceed the irrigation standard.

## Groundwater Facies and Source Identification

### Groundwater Type

The Piper trilinear diagram has been utilized to classify BAEA groundwater into different types of water based on the fundamental geochemical characteristics of ions concentrations (Fig. 7). By using this diagram, groundwater samples from the BAEA plain were classified into three distinct water types that correspond to Ca-Mg- $\text{SO}_4$ , mixed facies and Na-Cl water types.

In order to identify the different processes that control groundwater hydrochemistry, the Gibbs diagram (Fig. 8) was used by correlating the TDS with the weight ratios of ( $\text{Na}^+$  vs. ( $\text{Na}^+ + \text{Ca}^{2+}$ )) and the ratio of ( $\text{Cl}^-$  vs. ( $\text{Cl}^- + \text{HCO}_3^-$ )). The Gibbs diagram illustrates the relationship between water chemistry and the dominant processes controlling solute acquisition in the aquifer, such as rock weathering, evaporation, or atmospheric input.

The investigation of the relationship between water chemistry and the mineralogical composition of the studied aquifer system reveals that all groundwater samples fall in the field corresponding to the water-rock interaction, with the

Tab. 3 - Physico-chemical parameters of samples, water quality indices, descriptive statistic results, and standard limit of irrigation activity.

Tab. 3 - Parametri fisico-chimici dei campioni, indici di qualità dell'acqua, risultati della statistica descrittiva e valori legislativi di riferimento per l'utilizzo delle acque a scopo irriguo.

ID	Saturation Indicator		Irrigation Water Quality indices					
	Dolomite(d)	Gypsum	SAR	Na%	SSP	PS	RSC	IWQI
F04	1.34	-0.11	1.22	10.92	10.56	-6.51	-37.78	45
F05	1.88	-0.16	2.39	17.61	17.43	22.15	-45.50	18
F06	0.29	-0.64	1.76	21.20	20.58	7.63	-19.27	62
F07	0.67	-0.42	3.46	34.25	33.94	2.10	-19.17	58
P01	0.37	-0.16	2.90	21.55	21.37	21.48	-53.72	40
P02	1.09	-0.85	4.14	37.57	37.41	9.26	-15.85	48
F39	0.05	-1.28	5.40	54.42	54.22	9.95	-5.26	60
F40	0.33	-0.62	6.23	48.13	48.04	9.08	-15.64	44
F48	0.65	-1.51	3.02	34.03	33.80	15.05	-11.81	64
F49	0.33	-1.29	5.94	54.60	54.37	11.48	-6.84	53
P23	0.9	-1.17	0.02	26.66	0.33	3.85	-1.82	59
Minimum	1.88	-0.11	0.02	10.92	0.33	-6.51	-53.72	18
Maximum	0.05	-1.51	6.23	54.60	54.37	22.15	-1.82	64
Average	0.72	-0.75	3.32	32.81	30.19	9.59	-21.15	50.09
Standard Deviation	0.54	0.51	1.98	14.87	17.80	8.28	17.07	13.35
FAO*								

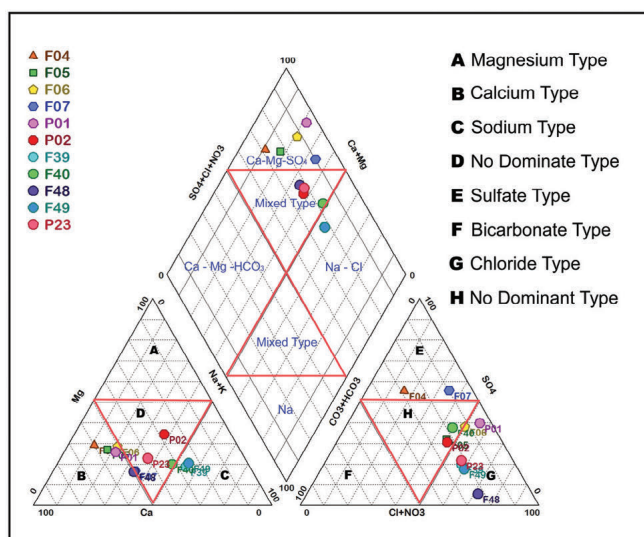


Fig. 7 - Piper diagram of the BAEA groundwater.

Fig. 7 - Diagramma di Piper delle acque sotterranee di BAEA.

exception of F04 and F05, which falls in the field dominated by evaporation. This may indicate that the dominant natural mechanism governing groundwater chemistry in the BAEA plain is closely related to the water-rocks interaction process and to a lesser but not negligible extent the evaporation. The ratios of  $(\text{Na}^+ / (\text{Na}^+ + \text{Ca}^{2+}))$  and  $(\text{Cl}^- / (\text{Cl}^- + \text{HCO}_3^-))$  vary from 0.17 to 0.71 and from 0.24 to 0.86, respectively. This suggests that calcium is replaced by sodium, and bicarbonate is replaced by chloride in the water, resulting mainly from the dissolution of evaporate minerals and/or the interaction with agricultural soils (Mandal et al., 2023). In addition, the samples, which are located in the upper part of the water-rock interaction zone, suggest that evaporation has an influence on the chemical composition of groundwater.

### Ion Exchange Processes

Ion exchange between water and clayey minerals is an important process that significantly impacts the hydrochemical composition of groundwater. The abundance of clay minerals in aquifer levels can play a crucial role in

determining the chemical composition of water. During this exchange process, clay minerals tend to balance their charge by fixing monovalent cations ( $\text{Na}^+$ ,  $\text{K}^+$ ) and releasing divalent cations ( $\text{Ca}^{2+}$ ,  $\text{Mg}^{2+}$ ) and vice versa.

The Chadha diagram (Fig. 9) for  $[(\text{Ca}^{2+} + \text{Mg}^{2+}) - (\text{Na}^+ + \text{K}^+)]$  and  $[\text{HCO}_3^- - (\text{SO}_4^{2-} + \text{Cl}^-)]$  shows that 82% of groundwater samples (9 samples) fall in the [D] zone, which reflects an inverse proportional relationship between monovalent and bivalent ions. The Ca-Mg- $\text{SO}_4/\text{Cl}$  water type corresponds to the samples affected by reverse ion exchange process, where sodium and potassium in the water are replaced by calcium and magnesium from the minerals. The waters from boreholes F49 and F39, located in the [C] field typical of saline water (Na-Cl), are influenced by direct cation exchange, where calcium and magnesium ions in the water are replaced by sodium and potassium from the clay minerals in the aquifer.

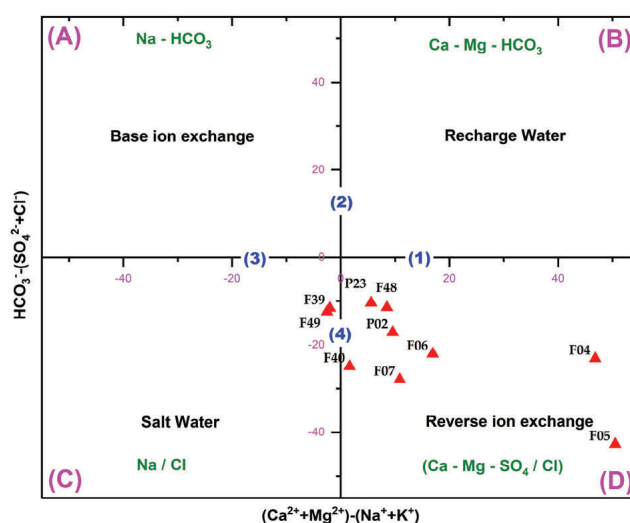
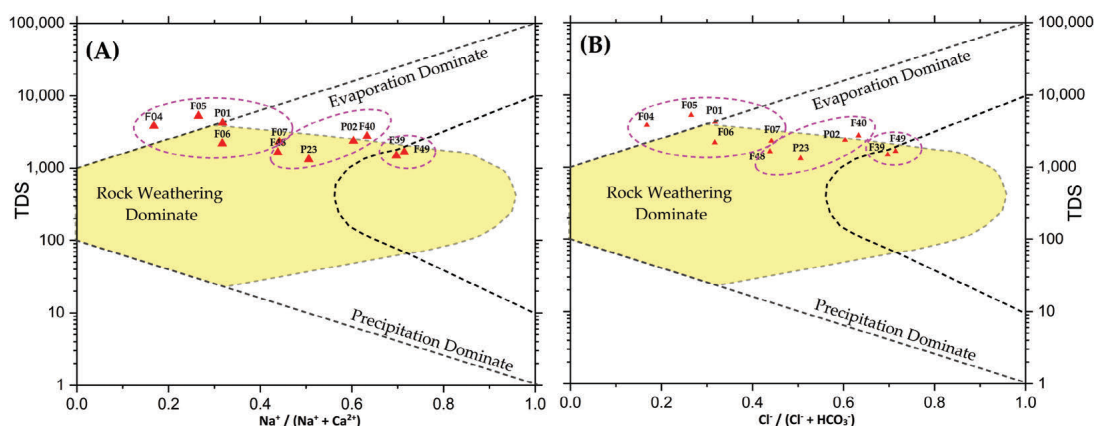


Fig. 9 - Chadha diagram of the BAEA aquifer groundwater: (1) alkaline earth metals exceed alkaline metals, (2) weak acidic anions exceed strong acidic anions, (3) alkaline metals exceed alkaline earth metals and (4) strong acidic anions exceed weak acidic anions.

Fig. 9 - Diagramma di Chadha delle acque sotterranee di BAEA: (1) i metalli alcalino-terrosi sono più abbondanti dei metalli alcalini, (2) gli acidi deboli sono più abbondanti degli acidi forti, (3) i metalli alcalini sono più abbondanti dei metalli alcalino-terrosi e (4) gli acidi forti sono più abbondanti degli acidi deboli.

Fig. 8 - Geochemical control processes with Gibbs diagrams: (A) TDS vs.  $(\text{Na}^+ / (\text{Na}^+ + \text{Ca}^{2+}))$ ; and (B) TDS vs.  $(\text{Cl}^- / (\text{Cl}^- + \text{HCO}_3^-))$ .Fig. 8 - Diagrammi di Gibbs per analizzare i processi geochimici: (A) TDS vs.  $(\text{Na}^+ / (\text{Na}^+ + \text{Ca}^{2+}))$ ; and (B) TDS vs.  $(\text{Cl}^- / (\text{Cl}^- + \text{HCO}_3^-))$ .

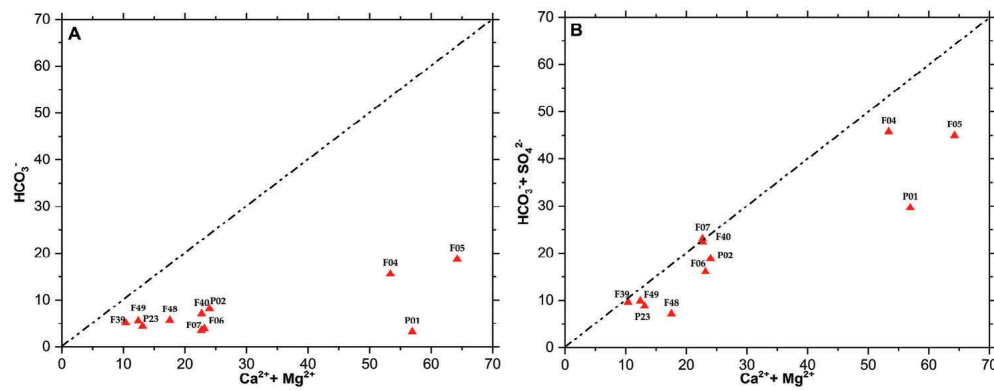


Fig. 10 - Diagrams (A)  $\text{HCO}_3^-$  vs  $(\text{Ca}^{2+} + \text{Mg}^{2+})$  and (B)  $(\text{Ca}^{2+} + \text{Mg}^{2+})$  vs  $(\text{HCO}_3^- + \text{SO}_4^{2-})$ .

Fig. 10 - Diagrammi (A)  $\text{HCO}_3^-$  contro  $(\text{Ca}^{2+} + \text{Mg}^{2+})$  e (B)  $(\text{Ca}^{2+} + \text{Mg}^{2+})$  contro  $(\text{HCO}_3^- + \text{SO}_4^{2-})$ .

The Chadha diagram is used to identify the hydrochemical evolution and water types as a function of anion and cation concentration. In addition, the scatter diagrams of  $(\text{Ca}^{2+} + \text{Mg}^{2+})$  vs  $(\text{HCO}_3^-)$  and  $(\text{Ca}^{2+} + \text{Mg}^{2+})$  vs  $(\text{HCO}_3^- + \text{SO}_4^{2-})$  show an excess of  $\text{Mg}^{2+}$  and  $\text{Ca}^{2+}$  relative to  $\text{HCO}_3^-$  and  $\text{SO}_4^{2-}$ . This pattern provides strong evidence of cation exchange with clay minerals (Fig. 10 A & B).

The  $[(\text{Ca}^{2+} + \text{Mg}^{2+}) - (\text{HCO}_3^- + \text{SO}_4^{2-})]$  vs.  $(\text{Na}^+ + \text{K}^+) - \text{Cl}^-]$  diagram shows that all the samples plot along a line with a slope of -1, highlighting the significant role played by cation exchange plays in shaping the chemical facies of groundwater (Fig. 11 (A)).

The relationship between  $(\text{Mg}^{2+}/\text{Ca}^{2+})$  and  $(\text{Mg}^{2+}/\text{Na}^+)$  can be used to determine the degree of leaching of salts from soils (Fig. 11 (B)). This is because the concentration of magnesium during the early stages of water evaporation does not increase due to the leaching of soil salts and does not decrease due to evaporation. The samples from the BAEA plain are clearly classified into three groups. The first group shows a low ratio  $(\text{Mg}^{2+}/\text{Na}^+)$  and a high ratio  $(\text{Mg}^{2+}/\text{Ca}^{2+})$ , suggesting an important influence of evaporation effect on the groundwater chemistry. The second group shows high  $(\text{Mg}^{2+}/\text{Na}^+)$  and  $(\text{Mg}^{2+}/\text{Ca}^{2+})$  ratios reflecting the significant contribution of water-rock interaction processes to the groundwater mineralization. The third group displays moderate ratios reflecting the combined influence of evaporation and the interaction of groundwater with the reservoir minerals.

The  $[(\text{Ca}^{2+} + \text{Mg}^{2+}) - (\text{HCO}_3^- + \text{SO}_4^{2-})]$  vs.  $(\text{Na}^+ + \text{K}^+) - \text{Cl}^-]$  diagram shows that all the samples plot along a line with a slope of -1, highlighting the significant role played by cation exchange plays in shaping the chemical facies of groundwater (Fig. 11 (A)).

The relationship between  $(\text{Mg}^{2+}/\text{Ca}^{2+})$  and  $(\text{Mg}^{2+}/\text{Na}^+)$  can be used to determine the degree of leaching of salts from soils (Fig. 11 (B)). This is because the concentration of magnesium during the early stages of water evaporation does not increase due to the leaching of soil salts and does not decrease due to evaporation. The samples from the BAEA plain are clearly classified into three groups. The first group shows a low ratio  $(\text{Mg}^{2+}/\text{Na}^+)$  and a high ratio  $(\text{Mg}^{2+}/\text{Ca}^{2+})$ , suggesting an important influence of evaporation effect on the groundwater chemistry. The second group shows high  $(\text{Mg}^{2+}/\text{Na}^+)$  and  $(\text{Mg}^{2+}/\text{Ca}^{2+})$  ratios reflecting the significant contribution of water-rock interaction processes to the groundwater mineralization. The third group displays moderate ratios reflecting the combined influence of evaporation and the interaction of groundwater with the reservoir minerals.

The USSL diagram is an effective tool for analyzing water quality for irrigation using electrical conductivity (EC) and sodium adsorption ratio (SAR) values (Fig. 12 (A)). The majority of groundwater samples belong to the class C3S1, which is characterized by high salinity with low sodium risk, reflecting that the water is not suitable for irrigation due to its high salinity content. Sample F40 belongs to the class C4S2,

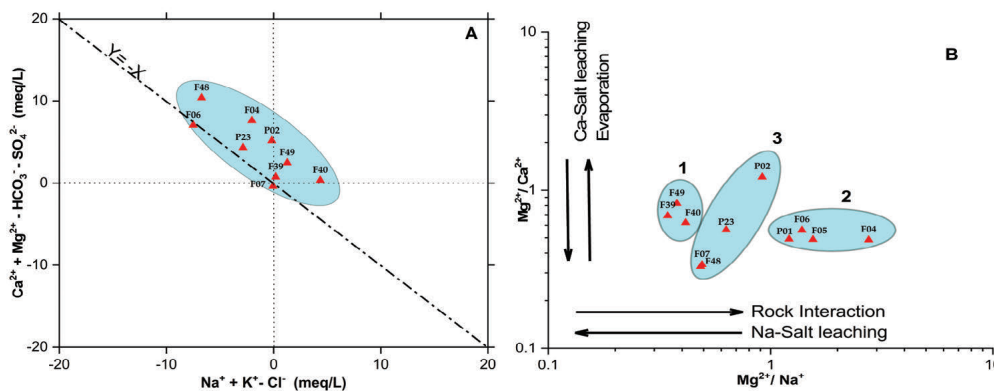


Fig. 11 - Diagrams of (A)  $(\text{Na}^+ + \text{K}^+ - \text{Cl}^-)$  vs  $(\text{Ca}^{2+} + \text{Mg}^{2+} - \text{HCO}_3^- - \text{SO}_4^{2-})$  and (B)  $(\text{Mg}^{2+}/\text{Na}^+)$  vs  $(\text{Mg}^{2+}/\text{Ca}^{2+})$ .

Fig. 11 - Diagrammi di (A)  $(\text{Na}^+ + \text{K}^+ - \text{Cl}^-)$  contro  $(\text{Ca}^{2+} + \text{Mg}^{2+} - \text{HCO}_3^- - \text{SO}_4^{2-})$  e (B)  $(\text{Mg}^{2+}/\text{Na}^+)$  contro  $(\text{Mg}^{2+}/\text{Ca}^{2+})$ .



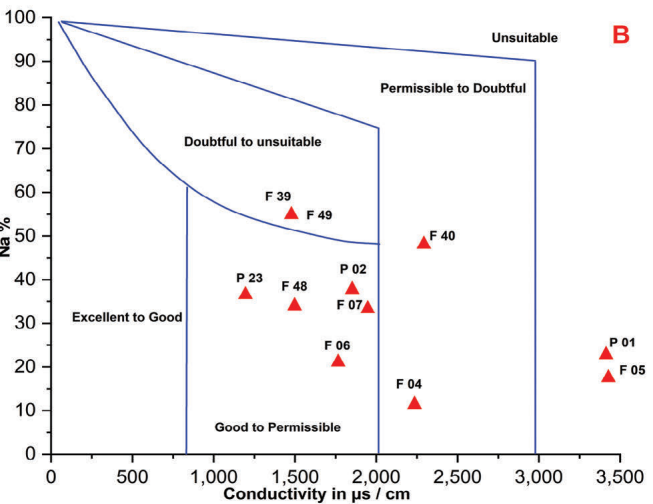
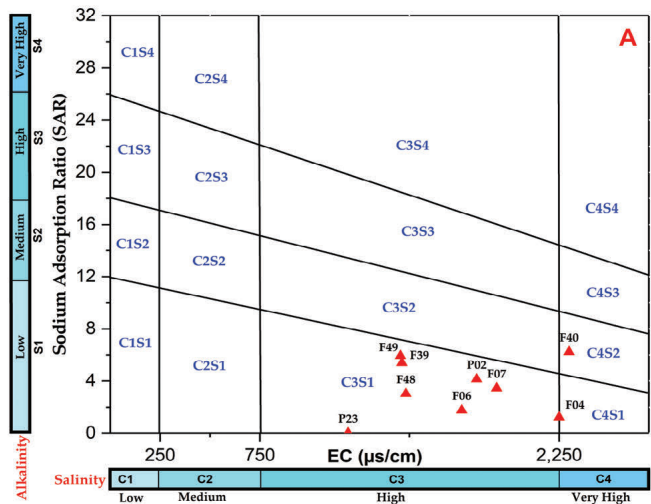


Fig. 12 - USSS and (B) Wilcox diagrams.  
Fig. 12 - Diagrammi (A) USSS e (B) di Wilcox.

highlighting very high salinization with medium sodium levels. Sample F4 lies between classes C3S1 and C4S1, showing fairly high salinity and low sodium concentration. Moreover, the Wilcox diagram (Fig. 12 (B)) allowed to classify BAEA groundwater samples into three categories with varying percentages such as 46% belonging to the class “Good to Permissible”, 18% to the class “Permissible to Doubtful”, 18% to the class “Doubtful and unsuitable” and 18% to the class “Unsuitable”. To simplify, “Excellent to Good” and “Good to Permissible” are grouped as “Good”; “Permissible To doubtful” as “Acceptable”; “Doubtful to unsuitable” as “Poor” and “Unsuitable” as “Bad” water.

The scatter plot of CAI values highlights that 4 samples have CAI values below 0 (Fig. 13). This suggests that significant exchanges between cations are taking place, especially in the eastern part of the BAEA plain. Six samples, which are located in the western part of the BAEA plain close to the Triassic outcrop of Djebel Ech Chehid, show positive CAI values indicating the aggressiveness of groundwater and its ability to dissolve limestone deposits.

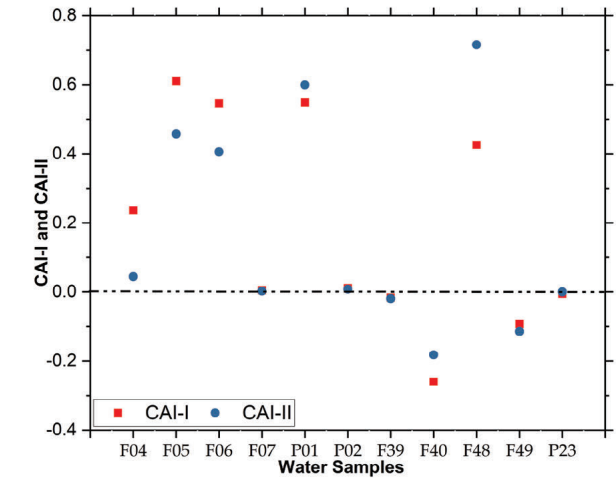


Fig. 13 - Chlor-Alkaline Indexes (CAI) diagram.  
Fig. 13 - Diagramma degli indici cloro-alcalini (CAI).

### Analysis Multivariate Statistics

#### Cluster Analysis (CA)

The Euclidean distance matrix, calculated for 9 hydrochemical parameters using Ward’s method, allowed us to classify the BAEA groundwater samples into three distinct groups (Fig. 14). The first group, which is characterized by very high TDS values (over 3000 mg/L), includes the water samples collected from the boreholes of the Sidi Ayyed region, near the Triassic series south of the Djebel Ech Chehid. It seems that the strong mineralization of the first group of groundwater samples is a result of the interaction with the salt formations of the Triassic. The second group consisting of groundwater samples with high  $K^+$ ,  $Mg^{2+}$  and  $NO_3^-$  contents suggests the effect of contamination processes related to anthropogenic activities, including fertilizer, insect killing, and herbicide in agricultural areas. The third group exhibits a wide range of ionic composition with high concentrations of  $SO_4^{2-}$ ,  $Cl^-$ ,  $HCO_3^-$ , Na and Ca reflecting a composition that may result from the water-rock interaction processes related to the dissolution of evaporates and carbonate minerals.

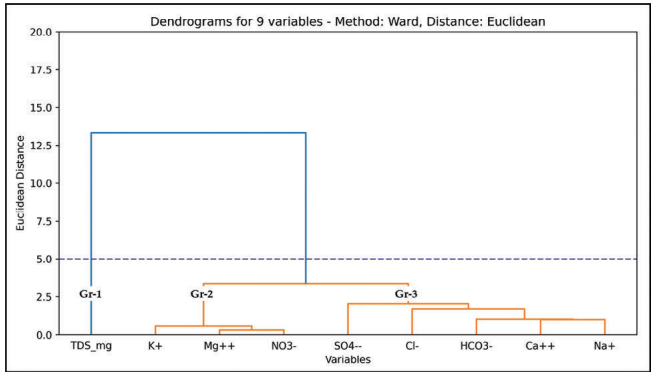


Fig. 14 - Clustered dendrogram of the BAEA groundwater.  
Fig. 14 - Dendrogramma dell’analisi di cluster effettuata per le acque sotterranee di BAEA.

### Factorial Analysis (FA) and Principal Component Analysis (PCA)

The factorial analysis indicates the relative weights assigned to each physico-chemical parameter following the application of Principal Component Analysis (PCA) combined with Centered Log-Ratio (CLR) transformation. These weights reflect the relative importance of the selected parameters and will be used to calculate the Irrigation Water Quality Index (IWQI). The weights obtained are: EC (0.352),  $\text{Na}^+$  (0.093),  $\text{Cl}^-$  (0.068),  $\text{HCO}_3^-$  (0.313), and SAR (0.174). These values highlight the predominant importance of electrical conductivity and bicarbonates suggesting that these two parameters contribute most significantly to irrigation water quality in the analyzed samples. These normalized weights, adjusted to ensure that their sum is exactly equal to 1 (Fig. 15), are then incorporated into the IWQI calculation formula (Equation 3) to comprehensively assess water quality for agricultural purposes.

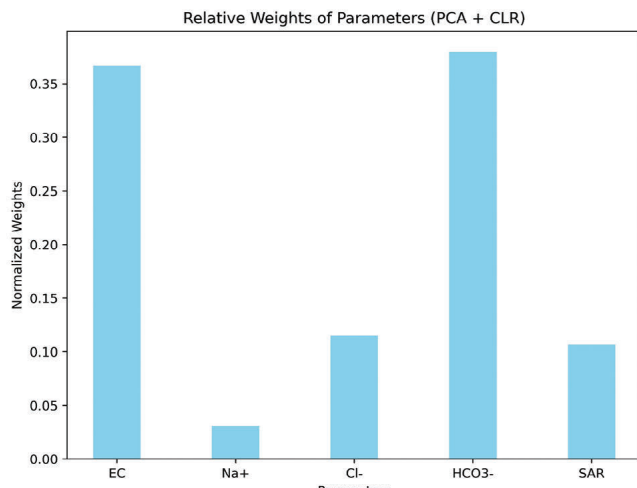


Fig. 15 - Standardized weights ( $W_i$ ) for the physico-chemical factors used to calculate IWQI according to equation (3).

Fig. 15 - Pesi standardizzati ( $W_i$ ) per i parametri fisico-chimici utilizzati per calcolare IWQI secondo l'equazione (3).

In order to assess the effectiveness of the principal component analysis (PCA), a correlation matrix and the KMO value were calculated. The correlation matrix for the eight parameters, which was used to determine the degree of contribution of each parameter to total mineralization, demonstrates that all variables are strongly correlated, with the exception of sodium. Several ratios including  $\text{Ca}^{2+}$  vs.  $\text{HCO}_3^-$ ,  $\text{Ca}^{2+}$  vs.  $\text{Mg}^{2+}$ ,  $\text{Ca}^{2+}$  vs.  $\text{SO}_4^{2-}$ ,  $\text{Ca}^{2+}$  vs. TDS and  $\text{K}^+$  vs.  $\text{SO}_4^{2-}$  show high correlation coefficients, with values exceeding 0.9 (Fig. 16).

However, there are also very weak or even negative correlations, of which  $\text{Na}^+$ ,  $\text{Cl}^-$ , and  $\text{K}^+$  can be cited as examples. The KMO value that was obtained is 0.53, which is higher than the threshold of 0.5, a commonly accepted minimum for PCA to be considered appropriate (Salem et al., 2023; B Patil et al., 2020).

The principal Component Analysis (PCA) was carried out using nine hydrochemical parameters ( $\text{Ca}^{2+}$ ,  $\text{Mg}^{2+}$ ,  $\text{Na}^+$ ,  $\text{K}^+$ ,  $\text{HCO}_3^-$ ,  $\text{Cl}^-$ ,  $\text{SO}_4^{2-}$ ,  $\text{NO}_3^-$ , and TDS) using 11 groundwater samples from the BAEA plain (Fig. 17). This approach has

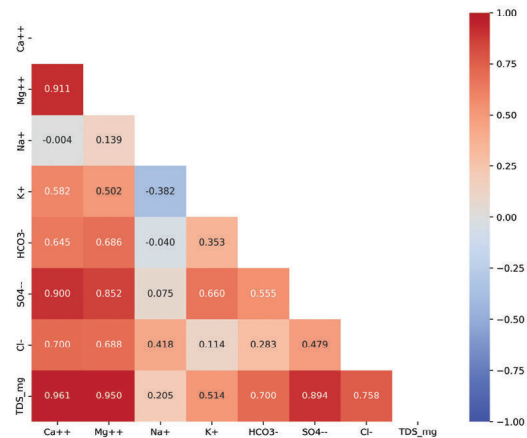


Fig. 16 - Correlation matrix for hydrochemical parameters.

Fig. 16 - Matrice di correlazione per i parametri idrochimici.

reduced the number of variables, making it possible to keep only the first two factors (F1 and F2) that exhibit the most important loading and exclude the less significant ones. The first two preserved factors, which display the highest variance, explain 82.7% of the total variance (63.27% for F1 and 19.43% for F2). In the variable space, F1 exhibits a strong correlation with all ions and TDS, which generally reflects the impact of natural processes on water salinization (Zare Farjoudi & Alizadeh, 2021). The position of the samples in the individual space shows that the samples F04, F05 and P01 are on the positive side of F1 confirming the involvement of interaction processes in the acquisition of groundwater mineralization mainly in the downstream part of the plain. The second group, which falls on the positive side of the F2 factor, includes samples influenced by the effects of dedolomitization and exchanges with clays that are relatively abundant in the study area. It includes samples with low salinity and located in areas dominated by carbonate formations and clays, mainly in the northern part of the study area. The third group, which lies on the negative side of F2, includes samples that are mainly found in agricultural regions and are strongly related to infiltration of irrigation water.

### The IWQI Classification

The IWQI, which will serve as a basis to quantify the impact of irrigation water on soil and crops, ranges from 18% to 64%, with an average of 50% (Tab. 3). This diversity of values suggests the multiple factors influencing water quality.

A study of the distribution of IWQI of the groundwater samples (Tab. 3) reveals an intriguing distribution. Indeed, 18% of samples display severe restriction, 36% high restriction, and 45% moderate restriction. The spatial distribution of the IQWI indices shows that 54% of samples, classified as severe and moderate restriction, are located in the south of the Triassic formation outcropping in the Djebel Ech Chehid and northwest of the Bou Arada region. This spatial distribution reflects the significant influence of the Triassic deposits and/or tectonic activities. These latter are represented by the TebourSouk and the Bou Arada faults (Arfaoui et al.,

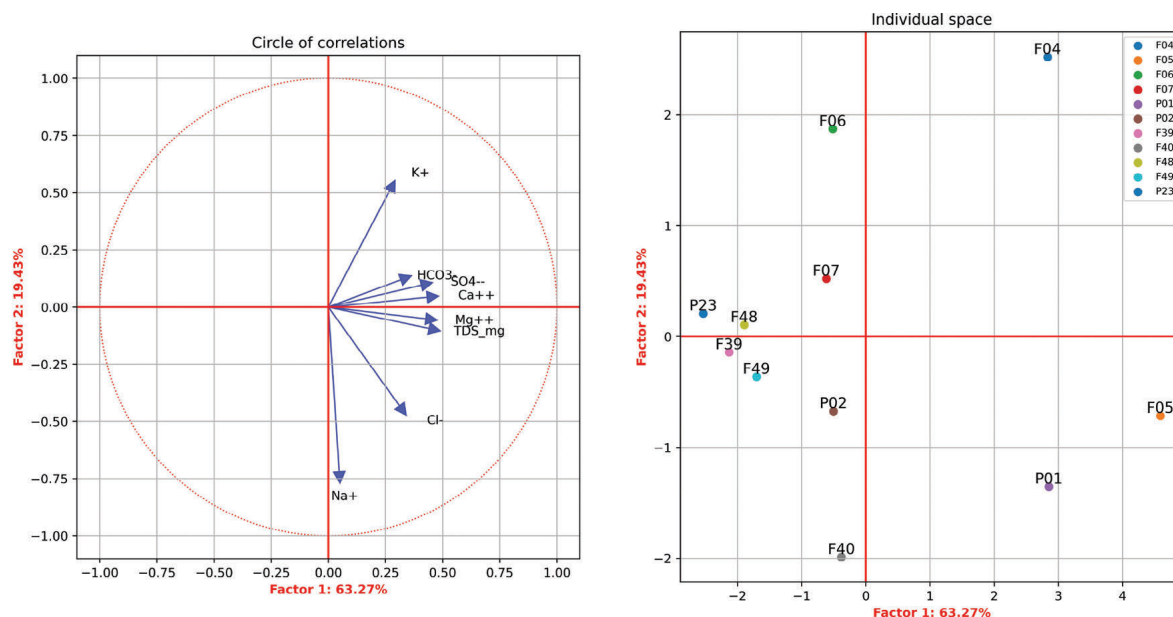


Fig. 17 - (A) Variable space deduced from the PCA; (B) main sample groups according to their scores for F1 and F2.

Fig. 17 - (A) Spazio delle variabili ottenuto dall'analisi PCA; (B) principali gruppi di campioni in base ai loro punteggi per F1 e F2.

2018; Ben Chelbi et al., 2013) which have a negative impact on groundwater quality, especially through the influx of deep waters of poor quality.

### Impact on Soil Composition

It is therefore essential to evaluate the suitability of water for irrigation using several indices, such as SAR, Na% and SSP. The calculated values of SAR, Na% and SSP range are from 0.02 to 6.2, and 10.9 to 54.6 and 0.33 to 54.4, respectively (Tab. 3). The resulting classification of these indices reflects an encouraging overview with 100% of samples falling into the excellent category for the SAR index, 73% of samples falling into the good to excellent category for Na% and 100% of samples classified as desirable for SSP (Tab.3). In spite of the positive irrigation water quality indicators, it is important to maintain vigilance and rigorous monitoring of water quality to prevent negative effects on soil and agricultural production. Thus, to ensure the sustainability of irrigation practices and the long-term health of the soil, it is necessary to introduce new approaches to assessing irrigation water quality (Arora et al., 2024; Salam et al., 2024).

### Precipitation of Alkali-Elements and RSC

In arid and semi-arid areas, excess of carbonate and bicarbonate as well as the abundance of bivalent cations such as  $\text{Ca}^{2+}$  and  $\text{Mg}^{2+}$  can create an ion imbalance leading to alkaline mineral precipitation, degrading the quality of irrigation water. This precipitation process is, firstly, accompanied by a considerable increase in the values of SAR and Na% and, secondly, by high values of RSC reflecting high levels of carbonate and bicarbonate ions, disrupting the physical properties of soil. According to the classification based on irrigation indices SAR, Na%, and SSP, the RSC index shows

values ranging from -53.12 to -1.82, with an average of -21.15 (Tab. 3) suggesting that the studied groundwaters are of good quality and suitable for irrigation practices.

### Geospatial analysis

Spatial distribution maps produced by interpolation of water quality indices are classified by the value intervals for each class (Tab. 4). IWQIs, which range from 18 to 64, were classified into 3 categories namely severe restriction, high restriction, and moderate restriction, each with the following weights 1, 2, and 3 respectively. Similarly, for the Na% and PS indices, the weights assigned are 5, 4, 3 and 5, 3, 1 respectively. For the SAR, SSP and RSC indices, the distribution of values is representative of a single class, which is assigned a weight of 5.

After data preparation, we move on to aggregating the raster's using the Raster Calculator tool to sum the raster's representative of the water quality indices. The resulting map shows the spatial distribution of these combined water quality indices ranging from 16 to 24 and corresponding to the sum of the index weights. This map, which has been reclassified to define 3 classes i.e. good, moderate and poor (Fig. 18), shows an intriguing spatial distribution. Poor-quality waters are located mainly to the east of the BAEA plain. Good quality water is found to the west of the BAEA plain, precisely to the south-west of Djebel Er Rihan, that corresponds to the main recharge area for the BAEA aquifer system. Water of moderate quality is found to the north of the Oued Er Rmil syncline. Spatial mapping of quality indices will enhance understanding of factors that impact water quality and reorient efforts towards sustainable management and groundwater resource protection.



Tab. 4 - Statistical analysis, IWQIs classification and weight reclassification.

Tab. 4 - Analisi statistica, classificazione degli IWQIs e riclassificazione pesata.

Index	Range	Class	Reclassify	Number of Samples
IWQI	85-100	No Restriction	5	
	70-85	Low Restriction	4	
	55-70	Moderate Restriction	3	5 (45%)
	40-55	High Restriction	2	4 (36%)
	0-40	Severe Restriction	1	2 (18 %)
SAR	< 10	Excellent	5	11 (100%)
	10 - 18	Good	4	
	19 - 26	Fair-to-Poor	3	
	> 26	Unsuitable	1	
Na%	< 20	Excellent	5	2 (18%)
	21 - 40	Good	4	6 (55%)
	41 - 60	Permissible	3	3 (27%)
	61 - 80	Doubtful	2	
	> 80	Unsuitable	1	
SSP	< 60	Suitable	5	11 (100%)
	> 60	Unsuitable	1	
PS	PS < 3	Excellent to Good	5	2 (18%)
	3 < PS < 5	Good to injurious	3	1 (9%)
	PS > 5	injurious to unsatisfactory	1	8 (73%)
RSC	< 1.25	Good	5	11 (100%)
	1.25 - 2.5	Doubtful	3	
	> 2.5	Unsuitable	1	

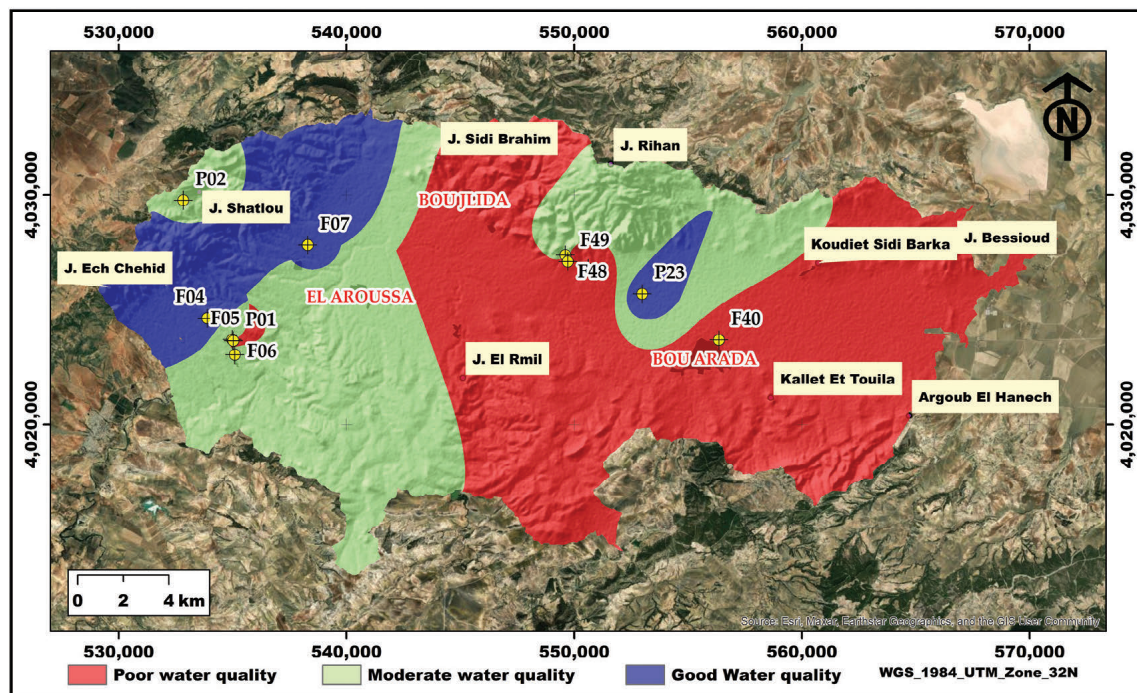


Fig. 18 - Spatial distribution of groundwater quality assessed after IWQIs aggregation.

Fig. 18 - Distribuzione spaziale della qualità delle acque sotterranee ottenuta dopo l'aggregazione degli IWQIs.

## Conclusion

The presented integrated approach, combining statistical analysis, geochemical interpretations and GIS mapping, provides consistent data for the development of sustainable groundwater resource management strategies in the BAEA region. A statistical study based on cluster and major component analyses revealed the existence of three water groups, which was confirmed by the Piper's diagram. This highlights the existence of three water facies including Ca-Mg-SO<sub>4</sub>, mixed facies and Na-Cl. Furthermore, the water hardness index (TH) revealed waters that fall within the category of hard brackish waters, which can lead to soil salinization and obstruction of irrigation systems.

The investigation of the relationship between TDS and the Na<sup>+</sup>/(Na<sup>+</sup>+Ca<sup>2+</sup>) and Cl<sup>-</sup>/(Cl<sup>-</sup>+HCO<sub>3</sub><sup>-</sup>) ratios confirms the strong contribution of water-rock interaction processes to groundwater salinization. The scatter plot of the samples according to the ionic ratios [(Ca<sup>2+</sup>+Mg<sup>2+</sup>)/(Na<sup>+</sup>+K<sup>+</sup>)] and [HCO<sub>3</sub><sup>-</sup>/(SO<sub>4</sub><sup>2-</sup>+Cl<sup>-</sup>)] shows that 82% of the groundwater samples are affected by reverse ion exchange processes. However, the F39 and F49 boreholes with different facies indicate that deep salt water rising along the Bou Arada fault is the principal cause of the water quality degradation in the eastern part of the plain.

In addition, the Mg<sup>2+</sup>/Ca<sup>2+</sup> and Mg<sup>2+</sup>/Na<sup>+</sup> relationships permit to classify groundwater samples into three groups, depending on the degree of influence of evaporation and/or water-rock interaction process. According to Wilcox's diagram, 9 samples fall under the category C3S1, which has a relatively high salinity. However, samples F4 and F40 fall under the categories C4S1 and C4S2, which have a very high salinity. The calculation of groundwater quality indices shows that the SAR, SSP and RSC values are typical for good water quality, while SP, Na% and IWQI have values spread over three water classes, ranging from excellent to poor quality. The spatial distribution of the water quality index combination is shown to have poor water quality in the eastern part of the BAEA plain and moderate water quality in the north of the Er Rmil syncline. The western part of the BAEA plain contains water of good quality. The deterioration in water quality in the eastern part of the BAEA plain can be attributed to the influence of faults, mainly the Bou Arada fault, which is responsible for the upwelling of poor-quality deep water. The passage of the Tébourouk fault near Djebel Bou Khil, in the Triassic formations, creates a breach in the sedimentary cover and causes an extremely salty surface water source to emerge to the north-west of the El Krib plain, with sodium concentrations in excess of 35 g/L and chlorine in excess of 66 g/L.

The results of this research provide a clearer picture of the quality levels of groundwater in the BAEA plain, guiding possible investigations and serving as a basis for the development of sustainable water resource management plans in the region. This holistic approach allows for an understanding of the complex factors influencing groundwater quality, going beyond simple assessments to provide decision

makers with the precise information needed to implement targeted interventions. Indeed, the resulting spatial analysis of water quality, combined with the identification of specific geochemical processes, facilitates the creation of appropriate strategies for sustainable irrigation practices, minimizing negative impacts on soil and crop yields while ensuring water resources availability.

## Acknowledgment

The authors are deeply indebted to the UFZ Helmholtz Centre for Environmental Research in Halle and their staff for their invaluable assistance with the hydrochemical analyses. Their expertise and efficient processing of our samples were critical to the successful completion of this research.

## Author contributions

Conceptualization, I.B.S.; fieldwork, I.B.S.; methodology, I.B.S., A.B.M. and S.G.; software, I.B.S.; validation, A.B.M. S.G. and I.T.; formal analysis, I.B.S.; investigation, A.B.M., S.G. and I.T.; resources, I.B.S.; data curation, I.B.S.; writing original draft preparation, I.B.S.; writing-review and editing, I.B.S., A.B.M. and S.G.; supervision, A.B.M. and S.G.; project administration, I.B.S.; All authors have read and agreed to the published version of the manuscript.

## Data Availability Statement

The authors declare that the data supporting the findings of this study are available within the paper. Should any raw data files be needed in another format they are available from the corresponding author upon reasonable request.

## Funding source

This study was not funded by any source.

## Competing interest

The authors declare no competing interests.

## Additional information

DOI: <https://doi.org/10.7343/as-2025-816>

Reprint and permission information are available writing to

[acquessotterranee@anipapozzi.it](mailto:acquessotterranee@anipapozzi.it)

Publisher's note Associazione Acque Sotterranee remains neutral with regard to jurisdictional claims in published maps and institutional affiliations.

## REFERENCES

- Abdelfattah, M., Abdel-Aziz Abu-Bakr, H., Aretouyap, Z., Sheta, M. H., Hassan, T. M., Geriesh, M. H., Shaheen, S. E.-D., Alogayell, H. M., M. EL-Bana, E. M., & Gaber, A. (2023). Mapping the impacts of the anthropogenic activities and seawater intrusion on the shallow coastal aquifer of Port Said, Egypt. *Frontiers in Earth Science*, 11, 1204742. <https://doi.org/10.3389/feart.2023.1204742>
- Abidi, J. H., Elzain, H. E., Sabarathinam, C., Selmane, T., Selvam, S., Farhat, B., Ben Mammou, A., & Senapathi, V. (2024). Evaluation of groundwater quality indices using multi-criteria decision-making techniques and a fuzzy logic model in an irrigated area. *Groundwater for Sustainable Development*, 25, 101122. <https://doi.org/10.1016/j.gsd.2024.101122>
- Adawe, A. M., Abdi, S. J., Abdi, A. M., & Omar, A. D. (2024). Water Quality Assessment of Groundwater Using Multivariate Statistical Techniques: A Case Study of Mogadishu, Banadir Region, Somalia. *American Journal of Environmental Protection*, 13(1), 19–29. <https://doi.org/10.11648/j.ajep.20241301.13>
- Amri, F. (1992). Étude par prospection électrique de la plaine El Aroussa-Bou Arda. “*Electrical prospecting study of the El Aroussa-Bou Arda plain*”. (p. 28) [Internal report]. Directorate general of water resources (DGRE).
- Appelo, C. A. J., & Postma, D. (2004). *Geochemistry, Groundwater and Pollution*. CRC Press. <https://doi.org/10.1201/9781439833544>
- Arfaoui, M. S., Khouni, R., Dridi, S., & Zargouni, F. (2018). Style and timing of tectonic deformation across the Bou Arada-El Fahs troughs system, Northeast Tunisia: Integration in the structural evolution of Atlas fold and thrust belt. *Arabian Journal of Geosciences*, 11(5), 95. <https://doi.org/10.1007/s12517-018-3436-3>
- Arora, P., Rani, N., & Anand, A. (2024). Assessment of Soil Quality of Rice Fields Under Irrigation with Different Water Sources. *Current Agriculture Research Journal*, 12(2), 694–704. <https://doi.org/10.12944/CARJ.12.2.15>
- Asma, B., & Şener, Ş. (2024). Appraisal of groundwater suitability and hydrochemical characteristics by using various water quality indices and statistical analyses in the Wadi Righ area, Algeria. *Water Supply*, 24(5), 1938–1957. <https://doi.org/10.2166/ws.2024.103>
- Azzouz, A. (1988). Étude de la prospection électrique dans la plaine de Bou Arada-El Aroussa. “*Electrical prospecting study on the Bou Arada-El Aroussa plain*”. (p. 34) [Internal report]. Directorate general of water resources (DGRE).
- B Patil, V. B., Pinto, S. M., Govindaraju, T., Hebbalu, V. S., Bhat, V., & Kannanur, L. N. (2020). Multivariate statistics and water quality index (WQI) approach for geochemical assessment of groundwater quality-A case study of Kanavi Halla Sub-Basin, Belagavi, India. *Environmental Geochemistry and Health*, 42(9), 2667–2684. <https://doi.org/10.1007/s10653-019-00500-6>
- Baird, R. B., & Eaton, A. D. (2017). *Standard Methods for the Examination of Water and Wastewater* (23rd ed.). American Public Health Association (APHA), of Water 678 Resource and Protection.
- Bakr, N. (2013). Sustainable natural resource management in regional ecosystems: Case studies in semi-arid and humid regions [Doctor of Philosophy, Louisiana State University and Agricultural and Mechanical College]. [https://doi.org/10.31390/gradschool\\_dissertations.806](https://doi.org/10.31390/gradschool_dissertations.806)
- Ben Chelbi, M., Kamel, S., Harrab, S., Rebaï, N., Melki, F., Meghraoui, M., & Zargouni, F. (2013). Tectonosedimentary evidence in the Tunisian Atlas, Bou Arada Trough: Insights for the geodynamic evolution and Africa-Eurasia plate convergence. *Journal of the Geological Society*, 170(3), 435–449. <https://doi.org/10.1144/jgs2012-095>
- Ben Yagoub, J. (1979). Contribution à l'étude géologique du jebel Rihane (Atlas tunisien). “*Contribution to the geological study of jebel Rihane (Tunisian Atlas)*”. (Note No. 13; pp. 5–17). National Mining Office (ONM).
- Besser, H., Redhaounia, B., Sana Bedoui, Ayadi, Y., Khelifi, F., & Hamed, Y. (2019). Geochemical, isotopic and statistical monitoring of groundwater quality: Assessment of the potential environmental impacts of the highly polluted CI water in Southwestern Tunisia. *Journal of African Earth Sciences*, 153, 144–155. <https://doi.org/10.1016/j.jafrearsci.2019.03.001>
- Bischoff, J. L., Juliá, R., Shanks, Iii, W. C., & Rosenbauer, R. J. (1994). Karstification without carbonic acid: Bedrock dissolution by gypsum-driven dedolomitization. *Geology*, 22(11), 995. [https://doi.org/10.1130/0091-7613\(1994\)022<0995:KWCABD>2.3.CO;2](https://doi.org/10.1130/0091-7613(1994)022<0995:KWCABD>2.3.CO;2)
- Bordbar, M., Busico, G., Sirna, M., Tedesco, D., & Mastroicco, M. (2023). A multi-step approach to evaluate the sustainable use of groundwater resources for human consumption and agriculture. *Journal of Environmental Management*, 347, 119041. <https://doi.org/10.1016/j.jenvman.2023.119041>
- Boukhalfa, K., Soussi, M., Ozcan, E., Banerjee, S., & Tounekti, A. (2020). The Oligo-Miocene siliciclastic foreland basin deposits of northern Tunisia: Stratigraphy, sedimentology and paleogeography. *Journal of African Earth Sciences*, 170, 103932. <https://doi.org/10.1016/j.jafrearsci.2020.103932>
- Chadha, D. K. (1999). A proposed new diagram for geochemical classification of natural waters and interpretation of chemical data. *Hydrogeology Journal*, 7(5), 431–439. <https://doi.org/10.1007/s100400050216>
- Clark, I. D., & Fritz, P. (1997). *Environmental isotopes in hydrogeology*. CRC Press/Lewis Publishers.
- CRDA. (2004). Carte Agricole de la région de Siliana. “*Agricultural map of the Siliana region*”. [Shapefile]. Tunisian Ministry of Agriculture; Regional Commissariat for Agricultural Development (CRDA) Siliana.
- Dali, T. (1994). Geological map of Gaafour No. 40 [Geological map]. National Mining Office (ONM), Directorate of Geology.
- Dali, T., Mahjoub, K., & Taamallah, N. (1999). Notice explicative de la carte géologique de Bou Arada n° 34. “*Explanatory note to the Bou Arada geological map No. 34*”. National Mining Office (ONM), Directorate of Geology.
- DGRE. (2019). *Annuaire d'exploitation des nappes 2018-2019*. “*Groundwater exploitation directory 2018-2019*”. (pp. 81–94) [Internal report]. Directorate general of water resources (DGRE).
- Doneen, L. D., University of California, Davis. D. of W. S. and E., & California. Department of Water Resources. (1964). Notes on Water Quality in Agriculture (Issue ptie. 1). Department of Water Science and Engineering, University of California, Davis. <https://books.google.tn/books?id=nBStYgEACAAJ>
- Eaton, F. M. (1950). Significance of carbonates in irrigation waters. *Soil Science*, 69(2), 123–134. <https://doi.org/10.1097/00010694-195002000-00004>
- ESRI. (2020). ArcGis Desktop (Version 10.8) [Computer software]. Environmental Systems Research Institute (ESRI). <https://www.esri.com>
- Fersi, M. (1979). Estimation du ruissellement moyen annuel sur les bassins du Sud-Est, du Sud-Ouest et du Sahel Sud, Tunis. “*Estimation of mean annual runoff in the South-East, South-West and South Sahel basins. Tunis*”. Water and Soil Resources Department (DRES).
- Gadelha, A. J. F., Rocha, C. O. D., Veras Neto, J. G., & Gomes, M. A. (2023). Multivariate statistical analysis of physicochemical parameters of groundwater quality using PCA and HCA techniques. *Ecletica Quimica*, 48(4), 37–47. <https://doi.org/10.26850/1678-4618eq.v48.4.2023.p37-47>
- Gallardo Ceron, F., West, J., Burke, I., Graham, J., & Colombero, L. (2023). Cluster Analysis for Hydrogeological Units Identification and Characterisation in Glaciofluvial Sediments. Fifth EAGE Conference on Petroleum Geostatistics, 1–5. <https://doi.org/10.3997/2214-4609.202335042>



- Garba, A., Idris, A. M., & Gambo, J. (2023). Groundwater Quality Assessment Using Principal Component and Cluster Analysis. In M. Sherif, V. P. Singh, A. Sefelnasr, & M. Abrar (Eds.), *Water Resources Management and Sustainability* (Vol. 121, pp. 335–346). Springer Nature Switzerland. [https://doi.org/10.1007/978-3-031-24506-0\\_22](https://doi.org/10.1007/978-3-031-24506-0_22)
- Gautam, A., Rai, S. C., Rai, S. P., Ram, K., & Sanny. (2022). Impact of anthropogenic and geological factors on groundwater hydrochemistry in the unconfined aquifers of Indo-Gangetic plain. *Physics and Chemistry of the Earth, Parts A/B/C*, 126, 103109. <https://doi.org/10.1016/j.pce.2022.103109>
- Guo, H., Gao, Z., & Xing, S. (2023). Water–Rock Interactions: Mineral Dissolution. In M. N. V. Prasad & M. Vithanage (Eds.), *Medical Geology* (1st ed., pp. 111–127). Wiley. <https://doi.org/10.1002/9781119867371.ch7>
- Hamzaoui-Azaza, F., Bouhlila, R., & Gueddari, M. (2012). Characterization of the mineralization of the Triassic water table (South-East Tunisia) by geochemical and statistical methods. 36, 49–62.
- Hartanto, P., & Lubis, R. F. (2023). Use the hot spring's Chloro-Alkaline Index (CAI) for the low enthalpy prospect of the Rawadanau geothermal field. *Journal of Physics: Conference Series*, 2596(1), 012049. <https://doi.org/10.1088/1742-6596/2596/1/012049>
- Hasbaia, M., Djerbouai, S., Khodja, H. D., Belazreg, N. E. H., Mitiche Kettab, R., & Ferhati, A. (2021). Hydrochemical analysis of groundwater quality in central Hodna Basin, Algeria: A case study. *International Journal of Hydrology Science and Technology*, 1(1), 1. <https://doi.org/10.1504/IJHST.2021.10040507>
- Henchiri, M., Abidi, M., & Jemmali, N. (2015). Large euhedral quartz crystals in the Triassic dolomites and evaporites of central Tunisia: Implications for silica diagenesis in sulphate-rich and high-Mg environments. *Arabian Journal of Geosciences*, 8(10), 8899–8910. <https://doi.org/10.1007/s12517-015-1788-5>
- Hunter, J. D. (2007). Matplotlib: A 2D Graphics Environment. *Computing in Science & Engineering*, 9(3), 90–95. <https://doi.org/10.1109/MCSE.2007.55>
- Jain, S., & Singh, Dr. P. (2022). A GIS-based Interpolation Technique to Predict Urban Ground Water Quality. *International Journal for Research in Applied Science and Engineering Technology*, 10(12), 528–538. <https://doi.org/10.22214/ijraset.2022.47928>
- Jausein, A., & Berthe, D. (1961). Geological map of J. Mansour No. 41 [Geological map]. National Mining Office (ONM), Directorate of Geology.
- Karar, A., & Henni, A. (2020). Scale Inhibition in Hard Water System. In A. M. Negm, A. Bouderbala, H. Chenchouni, & D. Barceló (Eds.), *Water Resources in Algeria—Part I* (Vol. 97, pp. 293–318). Springer International Publishing. [https://doi.org/10.1007/698\\_2020\\_530](https://doi.org/10.1007/698_2020_530)
- Kramer, I., & Mau, Y. (2023). Review: Modeling the Effects of Salinity and Sodicity in Agricultural Systems. *Water Resources Research*, 59(6), e2023WR034750. <https://doi.org/10.1029/2023WR034750>
- Li, R., Yan, Y., Xu, J., Yang, C., Chen, S., Wang, Y., & Zhang, Y. (2024). Evaluate the groundwater quality and human health risks for sustainable drinking and irrigation purposes in mountainous region of Chongqing, Southwest China. *Journal of Contaminant Hydrology*, 264, 104344. <https://doi.org/10.1016/j.jconhyd.2024.104344>
- Li, X. (2023). Combined cluster and discriminant analysis based on hydrochemical and isotopic evidence: A case study of the Yellow River Delta in China. *Advances in Computer and Engineering Technology Research*, 1(1), 12. <https://doi.org/10.61935/acetr.1.1.2023.P12>
- Mahjoub, K., & Dali, T. (1998). Geological map of Bou Arada No. 34 [Geological map]. National Mining Office (ONM), Directorate of Geology.
- Mandal, R., Das, A., Tripathy, G. R., Sudheer, A. K., Kumar, S., Deshpande, R. D., & Padhya, V. (2023). Impact of soil salinity on groundwater chemistry in semi-arid regions in Western India: Insights from major ion and stable isotopic  $\delta^2\text{H}$   $\text{H}_2\text{O}$ ,  $\delta^{18}\text{O}$   $\text{H}_2\text{O}$ , and  $\delta^{13}\text{C}$  DIC characteristics. *Groundwater for Sustainable Development*, 21, 100939. <https://doi.org/10.1016/j.gsd.2023.100939>
- Mandloi, S., Tagore, G. S., Kulhare, P. S., Nishant, K., Bangre, S., & Bangre, J. (2024). Fertility status of different soil associations of central India. *Annals of Plant and Soil Research*, 26(1), 148–158. <https://doi.org/10.47815/aprs.2024.10345>
- Mecibah, I., Medjani, F., Zahi, F., Djidel, M., Drouiche, A., Labar, S., & Hamilton, M.-L. (2024). Groundwater quality assessment using water quality indices and Gis within the Oued Guebli downstream subbasin (Collo plain, Northeastern Algeria). *Environmental Engineering and Management Journal*, 23(4), 755–770. <https://doi.org/10.30638/eemj.2024.059>
- Mehta, P., Jangra, M. S., Baweja, P. K., & Srivastav, A. L. (2024). Impact of climate change on rural water resources and its management strategies. In *Water Resources Management for Rural Development* (pp. 45–54). Elsevier. <https://doi.org/10.1016/B978-0-443-18778-0.00018-0>
- Meireles, A. C. M., Andrade, E. M. D., Chaves, L. C. G., Frischkorn, H., & Crisostomo, L. A. (2010). A new proposal of the classification of irrigation water. *Revista Ciência Agronômica*, 41(3), 349–357. <https://doi.org/10.1590/S1806-66902010000300005>
- Narvaez-Montoya, C., Mahlknecht, J., Torres-Martínez, J. A., Mora, A., & Bertrand, G. (2023, May 15). Coastal groundwater pattern recognition supported by cluster analysis. <https://doi.org/10.5194/egusphere-egu23-2876>
- Onumanyi, A. J., Molokomme, D. N., Isaac, S. J., & Abu-Mahfouz, A. M. (2022). AutoElbow: An Automatic Elbow Detection Method for Estimating the Number of Clusters in a Dataset. *Applied Sciences*, 12(15), 7515. <https://doi.org/10.3390/app12157515>
- Oueslati, M. N. (1990). Complément de prospection électrique dans la plaine de Bou Arda-El Aroussa. “Additional electrical prospecting on the Bou Arda-El Aroussa plain”. (p. 12) [Internal report]. Directorate general of water resources (DGRE).
- Ouhakki, H., El Fallah, K., & El Mejdoub, N. (2024). Spatiotemporal Interpolation of Water Quality Index and Nitrates using ArcGIS Pro for Surface Water Quality Modeling in the Oum Er-Rabia Watershed. *Ecological Engineering & Environmental Technology*, 25(5), 312–323. <https://doi.org/10.12912/27197050/186187>
- Pedregosa, F., Varoquaux, G., Gramfort, A., Michel, V., Thirion, B., Grisel, O., Blondel, M., Prettenhofer, P., Weiss, R., Dubourg, V., Vanderplas, J., Passos, A., Cournapeau, D., Brucher, M., Perrot, M., & Duchesnay, É. (2011). Scikit-learn: Machine Learning in Python. *Journal of Machine Learning Research*, 12(85), 2825–2830.
- Perthuisot, V. (1970). Geological map of Teboursouk No. 33 [Geological map]. Geology Department of the Ministry of Industry and Energy.
- Pham, N. Q., & Nguyen, G. T. (2024). Evaluating Groundwater Quality Using Multivariate Statistical Analysis and Groundwater Quality Index. *Civil Engineering Journal*, 10(3), 699–713. <https://doi.org/10.28991/CEJ-2024-010-03-03>
- Pierret, A., & Moran, C. J. (2011). Plant Roots and Soil Structure. In J. Gliński, J. Horabik, & J. Lipiec (Eds.), *Encyclopedia of Agrophysics* (pp. 628–632). Springer Netherlands. [https://doi.org/10.1007/978-90-481-3585-1\\_121](https://doi.org/10.1007/978-90-481-3585-1_121)
- Radmehr, A., Bozorg-Haddad, O., & Loáiciga, H. A. (2022). Integrated strategic planning and multi-criteria decision-making framework with its application to agricultural water management. *Scientific Reports*, 12(1), 8406. <https://doi.org/10.1038/s41598-022-12194-5>
- Ravikumar, P., Aneesul Mehmood, M., & Somashekar, R. K. (2013). Water quality index to determine the surface water quality of Sankey tank and Mallathahalli lake, Bangalore urban district, Karnataka, India. *Applied Water Science*, 3(1), 247–261. <https://doi.org/10.1007/s13201-013-0077-2>
- Rel Dechangue, T., & Kabeyene Veronique, K. (2023). Use Hydrochemistry and Environmental Isotopes for the Assessment Mineralization of Groundwater in Miopliocene Aquifers in Douala 3 (Cameroon). *American Journal of Water Resources*, 11(1), 11–19. <https://doi.org/10.12691/ajwr-11-1-2>
- Richards, L. A. (1954). Diagnosis and Improvement of Saline and Alkali Soils. *Soil Science*, 78(2), 154. <https://doi.org/10.1097/00010694-195408000-00012>

- Salam, S. B., S., & Kaushal, S. (2024). Soil management assessment framework for optimizing soil quality. *International Journal of Research in Agronomy*, 7(11), 01–06. <https://doi.org/10.33545/2618060X.2024.v7.i11a.1910>
- Salem, S., Gaagai, A., Ben Slimene, I., Moussa, A., Zouari, K., Yadav, K., Eid, M., Abukhadra, M., El-Sherbeeney, A., Gad, M., Farouk, M., Elsherbiny, O., Elsayed, S., Bellucci, S., & Ibrahim, H. (2023). Applying Multivariate Analysis and Machine Learning Approaches to Evaluating Groundwater Quality on the Kairouan Plain, Tunisia. *Water*, 15(19), 3495. <https://doi.org/10.3390/w15193495>
- Salman Dawood, A., Sagban Khudier, A., & Naeemah Bashara, A. (2018). Physicochemical Quality Assessment and Multivariate Statistical Analysis of Groundwater Quality in Basrah, Iraq. *International Journal of Engineering & Technology*, 7(4.20), 245. <https://doi.org/10.14419/ijet.v7i4.20.25934>
- Schoenherr, J., Reuning, L., Hallenberger, M., Lüders, V., Lemmens, L., Biehl, B. C., Lewin, A., Leupold, M., Wimmers, K., & Strohmenger, C. J. (2018). Dedolomitization: Review and case study of uncommon mesogenetic formation conditions. *Earth-Science Reviews*, 185, 780–805. <https://doi.org/10.1016/j.earscirev.2018.07.005>
- Singh, K. R., Goswami, A. P., Kalamdhad, A. S., & Kumar, B. (2020). Development of irrigation water quality index incorporating information entropy. *Environment, Development and Sustainability*, 22(4), 3119–3132. <https://doi.org/10.1007/s10668-019-00338-z>
- Smida, H., Abdellaoui, C., Zairi, M., & Ben Dhia, H. (2010). Cartographie des zones vulnérables à la pollution agricole par la méthode DRASTIC couplée à un Système d'information géographique (SIG): Cas de la nappe phréatique de Chaffar (sud de Sfax, Tunisie). "Mapping of areas vulnerable to agricultural pollution using the DRASTIC method coupled with a Geographic Information System (GIS): The case of the Chaffar water table (south of Sfax, Tunisia)". *Sécheresse*, 21(2), 131–146. <https://doi.org/10.1684/sec.2010.0246>
- Su, Q., Yu, H., Xu, X., Chen, B., Yang, L., Fu, T., Liu, W., & Chen, G. (2023). Using Principal Component Analysis (PCA) Combined with Multivariate Change-Point Analysis to Identify Brine Layers Based on the Geochemistry of the Core Sediment. *Water*, 15(10), 1926. <https://doi.org/10.3390/w15101926>
- Sun, W., Powell-Palm, M. J., & Chen, J. (2021). The geometry of high-dimensional phase diagrams: I. Generalized Gibbs Phase Rule (Version 3) [Mathematical Physics]. *arXiv*. <https://doi.org/10.48550/ARXIV.2105.01337>
- Sunkari, E. D., Abu, M., Zango, M. S., & Lomoro Wani, A. M. (2020). Hydrogeochemical characterization and assessment of groundwater quality in the Kwahu-Bombouaka Group of the Voltaian Supergroup, Ghana. *Journal of African Earth Sciences*, 169, 103899. <https://doi.org/10.1016/j.jafrearsci.2020.103899>
- Surkar, P. P., & Choudhary, M. K. (2023). Climate Change Impact Assessment on Water Resources—A Review. In P. V. Timbadiya, V. P. Singh, & P. J. Sharma (Eds.), *Climate Change Impact on Water Resources* (Vol. 313, pp. 113–125). Springer Nature Singapore. [https://doi.org/10.1007/978-981-19-8524-9\\_10](https://doi.org/10.1007/978-981-19-8524-9_10)
- Thapa, R., Gupta, S., & Kaur, H. (2020). Introducing an irrigation water quality index (IWQI) based on the case study of the Dwarka River basin, Birbhum, West Bengal, India. *Sustainable Water Resources Management*, 6(5), 86. <https://doi.org/10.1007/s40899-020-00450-3>
- User Manual HQd Portable Meter. (2020, Edition). Hach. HACH; DOC022.53.80017. <https://www.hach.com>
- Virtanen, P., Gommers, R., Oliphant, T. E., Haberland, M., Reddy, T., Cournapeau, D., Burovski, E., Peterson, P., Weckesser, W., Bright, J., Van Der Walt, S. J., Brett, M., Wilson, J., Millman, K. J., Mayorov, N., Nelson, A. R. J., Jones, E., Kern, R., Larson, E., ... Vázquez-Baeza, Y. (2020). SciPy 1.0: Fundamental algorithms for scientific computing in Python. *Nature Methods*, 17(3), 261–272. <https://doi.org/10.1038/s41592-019-0686-2>
- Ward, J. H. (1963). Hierarchical Grouping to Optimize an Objective Function. *Journal of the American Statistical Association*, 58(301), 236–244. <https://doi.org/10.1080/01621459.1963.10500845>
- Wu, J., & Sun, Z. (2016). Evaluation of Shallow Groundwater Contamination and Associated Human Health Risk in an Alluvial Plain Impacted by Agricultural and Industrial Activities, Mid-west China. *Exposure and Health*, 8(3), 311–329. <https://doi.org/10.1007/s12403-015-0170-x>
- Yıldız, S., & Karakuş, C. B. (2020). Estimation of irrigation water quality index with development of an optimum model: A case study. *Environment, Development and Sustainability*, 22(5), 4771–4786. <https://doi.org/10.1007/s10668-019-00405-5>
- Zare Farjoudi, S., & Alizadeh, Z. (2021). A comparative study of total dissolved solids in water estimation models using Gaussian process regression with different kernel functions. *Environmental Earth Sciences*, 80(17), 557. <https://doi.org/10.1007/s12665-021-09798-x>
- Zhang, Z., Yao, W., Huang, Y., Jiang, X., Gao, Z., Chen, S., & Tan, S. (2024). Irrigation Water Salinity Affects Solute Transport and Its Potential Factors Influencing Salt Distribution in Unsaturated Homogenous Red Soil. *Agronomy*, 14(11), 2453. <https://doi.org/10.3390/agronomy14112453>
- Zhu, X., Miao, P., Qin, J., Li, W., Wang, L., Chen, Z., & Zhou, J. (2023). Spatio-temporal variations of nitrate pollution of groundwater in the intensive agricultural region: Hotspots and driving forces. *Journal of Hydrology*, 623, 129864. <https://doi.org/10.1016/j.jhydrol.2023.129864>
- Zoller, U., Weintraub, O., & Havatselet, N. (1980). A chemical profile of recycled irrigation water in North-East Israel. *Science of The Total Environment*, 15(1), 51–64. [https://doi.org/10.1016/0048-9697\(80\)90084-4](https://doi.org/10.1016/0048-9697(80)90084-4)